Alternating Gradient Synchrotron Department
Relativistic Heavy Ion Collider Project
BROOKHAVEN NATIONAL LABORATORY
Upton, New York 11973

Spin Note

AGS/RHIC/SN No. 001
(January 19, 1996)

Conceptual Design for the Acceleration of Polarized Protons in RHIC

K. Brown (BNL), et al.

May 24, 1993
Revision 1: September 3, 1993
Revision 2: February 15, 1995

Conceptual Design for the Acceleration of Polarized Protons in RHIC [1]

K.Brown (BNL, AGS) G.Bunce (BNL, AGS) E.Courant (BNL, RHIC)
R.Fernow (BNL, CAP) R.Gupta (BNL,RHIC) S.Y.Lee (Indiana)
A.Luccio (BNL, AGS) Y.Makdisi (BNL, RHIC) S.Peggs (BNL, RHIC)
F.Pilat (BNL, RHIC) V.Ptitsin (Novosibirsk) L.Ratner (BNL, AGS)
T.Roser (Spokesperson, BNL, AGS) N.Tsoupas (BNL, RHIC)
Yu. Shatunov (Novosibirsk) H.Spinka (ANL) M.Syphers (Project Manager, BNL, AGS)
S.Tepikian (BNL, RHIC) A.G.Ufimtsev (IHEP) D.Underwood (ANL)
E.Willen (BNL, RHIC)

May 24, 1993
1. Revision: September 3, 1993
2. Revision: February 15, 1995

[1]Work was performed under the auspices of the U.S. Department of Energy and was supported by grants from the U.S. National Science Foundation

CONTENTS

1. INTRODUCTION

The Relativistic Heavy Ion Collider (RHIC) at Brookhaven allows for the unique possibility of colliding 250 GeV polarized proton beams at luminosities of up to $2\times10^{32}\,cm^{-2}s^{-1}$. This report describes the technical considerations of accelerating polarized proton beams in RHIC to a top energy of 250 GeV and of performing collisions of longitudinally and transversely polarized protons in the two interaction regions occupied by the PHENIX and STAR detectors.

Fig. 1 shows all the major components that are required for the acceleration of polarized beams to RHIC top energy. The feasibility of accelerating polarized protons in RHIC was the basis of the proposal the RHIC Spin Collaboration (RSC) submitted to the Brookhaven PAC in October 1992[1] and approved in 1993.

2. Polarized Ion Source, Booster and AGS

To achieve high luminosity, high energy polarized proton collisions in RHIC the intensity of the present AGS polarized proton source[2] is sufficient. The source produces about 35 μA of H^- with $75-80\%$ polarization in 350 μs pulses at a repetition rate of 5 Hz. The polarized H^- ions are accelerated to 200 MeV with an RFQ and the 200 MHz LINAC with an efficiency of about 50%. Twenty pulses of H^- ions are strip-injected, accumulated, and captured into a single bunch in the AGS Booster with an estimated efficiency of about 50%. The bunch in the Booster will then contain $N_B = 4 \times 10^{11}$ polarized protons with a normalized emittance of about $\epsilon_N = 10\pi$ $mm\ mrad$. The single bunch of polarized protons is accelerated in the Booster to 1.5 GeV kinetic energy and then transferred to the AGS, where it is accelerated to 25 GeV .

During acceleration, the polarization may be lost when the spin precession frequency passes through a depolarizing resonance. These resonances occur when the number of spin precession rotations per revolution $G\gamma$ ($G = 1.793$ is the anomalous magnetic moment of the proton, $\gamma = \frac{E}{m}$) is equal to an integer (imperfection resonances) or equal to $kP \pm \nu_y$ (intrinsic resonances). Here $P = 12$ is the superperiodicity of the AGS, $\nu_y = 8.8$ is the vertical betatron tune and k is an integer. The depolarization is caused by the small horizontal magnetic fields present in all ring accelerators which, at the resonance condition, act coherently to move the spin away from the stable vertical direction. Imperfection resonances are due to the horizontal fields caused by the vertical closed orbit errors and intrinsic resonances are caused by the horizontal focusing fields which are sampled due to the vertical betatron motion. The two resonances in the Booster ($G\gamma = 3$ and $G\gamma = 4$) are too weak to cause any significant depolarization. Traditionally, the depolarizing resonances in the AGS were corrected by the tedious harmonic correction method for the imperfection resonances and the tune jump method for the intrinsic resonances[3].

Two polarized beam test runs of experiment E-880 at the AGS have recently demonstrated the feasibility of polarized proton acceleration using a 5% partial Siberian Snake[4]. During the first run[5] in April 1994 it was shown that a 5% Snake is sufficient to avoid depolarization due to the imperfection resonances without using the harmonic correction method. The upper part of Fig. 3 shows the evolution of the beam polarization as the beam energy and therefore $G\gamma$ is increased. As predicted the polarization reverses the sign whenever $G\gamma$ is equal to an integer. The lower part of Fig. 3 shows that no polarization was lost at the imperfection resonances. The only polarization loss occurred at the location of the intrinsic resonances for which the pulsed quadrupoles are required for the tune jump method. During the first run the pulsed quadrupoles were not available. During the second run in December 1994 it was shown that it is possible to use the tune jump method in the presence of the partial Snake. A new record energy for accelerated polarized beam of 25 GeV was reached with about 12 % beam polarization left. Again no polarization was lost due to the imperfection resonances and depolarization from most imperfection resonances was avoided with the tune jump quadrupoles. However, as can be seen from Fig. 4, which shows the achieved polarization as a function of beam energy, significant amount of polarization was lost at $G\gamma = 12 + \nu_y$ and $G\gamma = 36 + \nu_y$. The first of these two resonances was successfully crossed previously and it will require further study to explain the unexpected polarization loss during the December run. The strength of the tune jump quadrupoles is not sufficient to jump the second resonance. We attempted to induce spin flip at this resonance but were only partially successful. During the next study run the method of inducing spin flip at intrinsic resonances will be further investigated. Table 2.1 summarizes the polarized proton beam parameters achieved in the AGS and also the requirements for RHIC.

At 25 GeV, the polarized protons are transferred to RHIC. At this energy the transfer line between the AGS and RHIC is spin transparent[6]. If the last resonance, $G\gamma = 36 + \nu_y$, cannot be crossed without significant polarization loss it is possible to transfer the polarized protons to RHIC before crossing this resonance in the AGS at an energy of 22.4 GeV ($\gamma \approx 25$). This is discussed in the following chapter.

We estimate that the overall efficiency of the acceleration and beam transfer is better than 50%, giving 2×10^{11} protons per bunch. With proper care in the tune jump procedure the normalized emittance of the bunch is expected to be less than 20π $mm\ mrad$. We repeat the process until all 114 bunches of each ring are filled. Since each bunch is accelerated independently, we have the option of preparing the polarization direction of each bunch independently. Filling both RHIC rings with 114 bunches each and acceleration to full energy will only take about 10 minutes which is short compared to the expected lifetime of the stored polarized proton beams in RHIC of many hours.

	Intensity	Polarization	Emittance	Momentum
1988	1.8×10^{10}	65 %		up to $13.3\,GeV/c$
		42 %		up to $21.7\,GeV/c$
1994	0.5×10^{10}	64 %	$30\pi\,mm\,mrad$	up to $10.7\,GeV/c$
		31 %	$30\pi\,mm\,mrad$	up to $23.3\,GeV/c$
		12 %	$30\pi\,mm\,mrad$	up to $25.4\,GeV/c$
RHIC	$2-4 \times 10^{11}$	$70-80$ %	$10-20\,\pi\,mm\,mrad$	up to $25.4\,GeV/c$

Table 2.1: AGS polarized beam parameters. The 1988 data reflects the result of the many year effort to accelerate polarized beam in the AGS using pulsed quadrupoles and numerous correction dipoles. The 1994 date comes from the first two test runs of E-880 testing the Parital Siberian Snake in the AGS. The RHIC data shows the required beam parameters for the RHIC spin program.

3. AGS-TO-RHIC TRANSFER LINE

The AGS to RHIC (ATR) transfer line[7] has been designed to transport a proton beam in a range of energies, with maximum energy of 29.05 GeV. which corresponds to a value of $G\gamma = 57.32$ [$G = (g-2)/2 = 1.7928$, g is the gyromagnetic ration of a proton]. The relative location of the horizontally and vertically bending magnetic elements of the (ATR) line is such that the line will affect the polarization of a fully polarized AGS proton beam at the RHIC injection point. In this chapter, which is based on previous work[6], we calculate the polarization of a proton beam as a function of proton energy at the injection point, and we determine the optimum injection proton energy for maximum beam polarization at this point.

3.1. ATR Sections Affecting the Proton Beam Polarization

A schematic diagram of the ATR line shows in Fig. 5. In this part of the report we briefly describe the various sections of the ATR line which may have an effect upon the polarization of the proton beam:

1. *Horizontal bend of* 4.25° : Has almost no effect on a vertically polarized beam. The polarization of the protons with off-median plane trajectories is affected by the fringe field of the magnet by less than 0.01%. In the calculations, this effect as well as the effect of the fringe field of all the uniform field dipoles and all the quadrupoles is included.

2. *Horizontal bend of* 8°: This section consists of a set of four combined function magnets, and has a very small effect on the polarization of protons with off axis trajectories. This effect is included in the calculations of this study.

3. A schematic diagram of the 20° bend section is shown in Fig. 6. It consists of two 2.5° combined function horizontally bending magnets, followed by a 12.5 $mrad$ vertically bending magnet and six 2.5° combined function magnets which bend the beam at the new (x,z) plane (see Fig.2), and finally a 12.5 $mrad$ vertically bending magnet which restores the beam in the original horizontal plane.

4. *The* 90° *big bend:* It consists of 29 combined function magnets followed by a uniform field dipole. This section has no effect on a fully vertically polarized beam, however it does have a modulating effect on a beam which is not vertically polarized (see Results section.)

5. A schematic diagram of the injection section shows in Fig.7. A brief explanation of the various magnetic elements of this section appears in this figure. In the context of this report we define as "injection point", the point at the exit of the injection kicker. We also assume that all the RHIC magnetic elements which appear in Fig. 7, have their symmetry axes lying on the RHIC plane.

The coordinate system used in this study is: x-radial, y-vertical, z-along beam.

3.2. Spin Orientation at RHIC Injection

The calculations to determine the spin orientation at the injection point were based on the numerical integration of two equations: the differential equation of motion (Eq. 3.1) of a charged particle moving in static magnetic and electric fields, and the spin precession equation (Eq. 3.2) of particle with magnetic moment in the same electric and magnetic field:

$$\frac{d\mathbf{v}}{dt} = \frac{e}{m\gamma}\left(\mathbf{v}\times\mathbf{B} + \mathbf{E} - \frac{(\mathbf{v}\cdot\mathbf{E})\,\mathbf{v}}{c^2}\right) \tag{3.1}$$

$$\frac{d\mathbf{s}}{dt} = \frac{e}{m\gamma}\left((G\gamma+1)\,\mathbf{s}\times\mathbf{B} + (\gamma-1)\,G\frac{(\mathbf{v}\cdot\mathbf{B})\,(\mathbf{v}\times\mathbf{s})}{v^2} + \left(G\gamma + \frac{1}{1+\frac{1}{\gamma}}\right)\frac{\mathbf{s}\times(\mathbf{E}\times\mathbf{v})}{c^2}\right) \tag{3.2}$$

The computer code which performs these calculations comes under the name RSPIN and is a modified version of the RAYTRACE computer code.

3.2.1. Results

The results of the calculations are shown in figures 8, 9, and 10. Fig. 8 shows the directional cosines of the spin vector at the entrance of the switching magnet as a function of the particle γ, for particles along the central trajectory. The maximum polarization in front of the switching magnet occurs at $\gamma = 26.75$ Fig. 9 is a plot of the same physical quantities as in Fig. 8 but at the location of the injection point as defined in Fig. 7. The frequent variation of the directional cosines S_x and S_z as a function of γ is due to the spin precession of the particle in the 90° big bend. Fig. 9 shows that the proton polarization is above 98 % for $\gamma \approx 26.5$, and falls to just above 90 % at $\gamma = 25.1$ and $\gamma = 27.8$. Thus the proton energy range corresponding to these two limits of values may be an acceptable energy range for polarized beam injection into RHIC. Finally Fig. 10 shows the directional cosines of the spin vector at the injection point for an off-central ray. The coordinates of this ray at the origin of the ATR line were selected based on a normalized 95% beam emittance $\varepsilon = 20\pi\, mm\, mrad$, and on the beam parameters also at the origin of the ATR line for $\gamma \approx 26$. Comparing the results from Fig.9 (for a central ray) with the results from Fig. 10 (for off-central ray) we conclude that the effect of the fringe fields of the magnetic elements and the effect of the quadrupoles on the beam polarization at the injection point is not significant.

3.2.2. Increased Energy Range for Spin Transparent AGS-to-RHIC Transfer Line

From the preceding section we conclude that the ATR beam transfer line can transfer a fully polarized AGS beam in the energy range which corresponds to $\gamma_{min} = 25.1$ and $\gamma_{max} = 27.8$ with 0 to 10 % depolarization depending on the energy. In this section we suggest a way to "tune" the ATR transfer line for minimum depolarization at the injection point and for a wider energy range. A schematic diagram of the proposed method shows in Fig. 11 where three dipole magnets have been added to the ATR beam line. The first of the three dipoles is placed in front of the second $12.5\, mrad$ vertically bending magnet of the 20° bend of the ATR line (see Fig. 6) Its function is to precess the proton spin by the required angle about the y-axis so that the vertical bending magnet restores the spin along the y-axis of the coordinate system after the vertical bending magnet. The other two dipoles in Fig. 11 will restore the beam trajectory and also cancel out the horizontal dispersion introduced by the first dipole. The first and third dipoles are identical with a 1 meter length and maximum operating field of $1.4\, T$ and the second magnet has two meter length and the same operating field as the first and third magnets. By exciting these three magnets with the proper field one can "tune" the beam line for minimum depolarization at the injection point for a given proton beam energy. Fig. 12 shows the spin orientation at the RHIC injection point in the energy range corresponding to $\gamma = 22$ and $\gamma = 28$. To obtain the results shown in Fig. 12 the three magnets, mentioned above, were excited to provide maximum polarization of a proton beam with $\gamma = 25$ at the entrance of the switching magnet. From Fig. 12 we also see that polarization of over 90 % can be obtained at the RHIC injection point for an energy range corresponding to $\gamma_{min} = 23.2$ and $\gamma_{max} = 27$.

4. Siberian Snakes and Spin Rotators in RHIC

4.1. General Lay-out

By inserting two full Siberian Snakes on opposite sides of each of the two RHIC rings, depolarization from imperfection and intrinsic depolarizing resonances can be avoided up to the top energy of 250 GeV. In addition to the Siberian Snakes, spin rotators are required at the intersection points used by PHENIX and STAR to allow for measurements of spin effects with longitudinally polarized protons. The spin rotators rotate the polarization from the vertical direction into the horizontal plane on one side of the interaction region and restore it to the vertical direction on the other side.

The Siberian Snakes introduce a 180° spin rotation without generating a net orbit distortion. The spin rotators placed around the experiments rotate the spin by 90° to provide longitudinal polarization at the interaction region again without generating net orbit distortions. In both cases the spin rotation is accomplished with a sequence of constant field, superconducting helical dipole magnets.

Each Snake rotates the spin by 180° around a horizontal axis and the two axes of the two Snakes of each ring have to be perpendicular on each other. We are planning to use pairs of Siberian Snakes with one Snake rotating the spin around an axis that points 45° to the outside and the other Snake rotating around an axis that points 45° to the inside of the ring. In this case all Snakes can be constructed in same way. Also, the two Snakes of each ring have to be installed on opposite sides of the ring. In fact, the beam direction in one Snake has to be exactly opposite to the beam direction in the other Snake to within $0.3\,mrad$.

The following is a summary for the locations and construction of the Siberian Snakes and the spin rotators (see Fig. 1):

- Two pairs of full Siberian Snakes, one pair in each ring, are installed at the 4 o'clock and 10 o'clock regions as shown in Fig. 2. These Snakes rotate the spin around axes that point 45° to the inside or outside of the ring. We are planning to install the Siberian Snakes in the $13\,m$ long, cold straight sections between Q7 and Q8.

- The two pairs of spin rotators, one set for PHENIX at the 8 o'clock region and another set for STAR at the 6 o'clock region, are installed in the $40\,m$ long straight sections between Q3 and Q4 on either side of the interaction region. The beam direction in the straight sections is different from the direction in the collision area by $3.67\,mrad$ which introduces a spin rotation that is larger by a factor of $G\gamma$. This means that the spin rotators have to prepare a horizontal polarization direction such that after this spin rotation the desired longitudinal polarization direction is obtained at the interaction point.

4.2. Siberian Snake and Spin Rotator Design

For both the Siberian snakes and the spin rotators we are planning to use four helical magnets[8]. Helical field magnets have some distinctive advantages over more conventional transverse snakes or rotators: (i) the maximum orbit excursion is smaller, (ii) orbit excursion is independent from the separation between adjacent magnets, and (iii) they allow an easier control of the spin rotation and the orientation of the spin precession axis.

In each magnet, in principle the transverse magnetic field should rotate a full 360° as one progresses to the other side. In this case however, if the fringe field is taken into account, the field integrals cannot be made equal to zero. The result is that a particle entering in the magnet on axis will not in general emerge on axis. In our design we have solved the problem by making the field rotation somewhat less than 360°, so the field integrals can be exactly compensated at least for one beam energy. Moreover, in order to simplify the construction of the snakes/rotators, a solution has been worked out with all magnetic modules identical in both devices. The only variation is that the helix of some magnets is right-handed and of some left-handed.

Snake parameters are listed in Table 4.1. The parameters are a result of an optimization using a three dimensional orbit and spin tracking program that includes the effects of fringe fields[9]. The result of the orbit and spin tracking is shown in Fig. 13. All helical magnets are powered by separate power supplies. This allows for an adjustment of

Number of helical magnets				4
Total length				$10.56\,m$
Magnet bore				$100\,mm$
Helical Magnets				
	Length	Field twist	Field orientation	Field strength
1	$2.40\,m$	$+345°$	$7.5°$	$1.191\,T$
2	$2.40\,m$	$+345°$	$187.5°$	$3.864\,T$
3	$2.40\,m$	$+345°$	$7.5°$	$3.864\,T$
4	$2.40\,m$	$+345°$	$187.5°$	$1.191\,T$
Max. orbit excursion ($25\,GeV$) (hor./ver.)				$14.7\,mm\,/\,31.5\,mm$
Total field intergral				$24.3\,Tm$
Orbit lengthening				$1.82\,mm$

Table 4.1: Parameters for the Siberian Snake magnets. "+" of field twist stands for a right-handed helix, "-" stand for a left-handed helix. The column 'Field orientation' gives the magnetic field direction at the entrance of the magnet measured counter-clockwise from the vertical direction.

Number of helical magnets				4	
Total length				$10.56\,m$	
Magnet bore				$100\,mm$	
Helical Magnets					
	Length	Field twist	Field orientation	Field ($25\,GeV$)	Field ($250\,GeV$)
1	$2.40\,m$	$+345°$	$97.5°$	$2.047\,T$	$3.378\,T$
2	$2.40\,m$	$-345°$	$82.5°$	$2.654\,T$	$3.141\,T$
3	$2.40\,m$	$+345°$	$97.5°$	$2.654\,T$	$3.141\,T$
4	$2.40\,m$	$-345°$	$82.5°$	$2.047\,T$	$3.378\,T$
Max. orbit excursion ($25\,GeV$) (hor./ver.)				$24.1\,mm\,/\,10.0\,mm$	
Total field intergral				$22.6\,Tm$	
Orbit lengthening				$1.25\,mm$	

Table 4.2: Parameters for the spin rotator magnets. "+" of field twist stands for a right-handed helix, "-" stand for a left-handed helix. The column 'Field orientation' gives the magnetic field direction at the entrance of the magnet measured counter-clockwise from the vertical direction. The magnetic field strengths are caluculated for longitudinal polarization at the beam collision point.

the spin tune to 1/2 and of the direction of the rotation axis to compensate for the effect of the detector solenoids. This is shown in Fig. 14.

Spin rotator parameters are listed in Table 4.2. The result of the orbit and spin tracking is shown in Fig. 15. Since in RHIC the direction of the spin rotator beam line is at an horizontal angle $\theta = 3.674$ mrad with the direction of the adjacent insertion, in order to obtain a longitudinal polarization at the insertion the spin should emerge from the rotator in the horizontal plane and at an angle $G\gamma\theta$ with the rotator axis. The needed rotation is therefore dependent on the beam energy. The values of the field needed to provide a longitudinal polarization at different energies are shown in Fig. 16.

4.3. Effect on Lattice

Calculations of the changes to the RHIC lattice parameters were performed using MAD. It is worth noting that the survey algorithm in MAD does not work properly since the Snakes introduce torsion into coordinate system. The following changes in the lattice parameters are caused by the introduction of two Snakes, each located between Q7 and Q8 as described above:

Comment	ν_x	ν_y	$D_x^{\max}$	$D_y^{\max}$	β_x^*	β_y^*
No Snakes	28.827	28.823	$1.674\,m$	0	$2.0\,m$	$2.0\,m$
With Snakes, Injection energy	28.837	28.836	$1.738\,m$	$0.110\,m$	$2.0\,m$	$2.1\,m$
With Snakes, Top energy	28.827	28.823	$1.678\,m$	$0.009\,m$	$2.0\,m$	$2.0\,m$

Clearly the changes of the lattice parameters are very small and can easily be corrected for.

4.4. Compensation for Detector Solenoids

The STAR and PHENIX detectors use solenoid magnets as spectrometers. With transverse polarization at the collision point the solenoid contributes to the imperfection resonance strength,

$$\epsilon_{imp,sol} = \frac{1+G}{2\pi}\frac{\int B_{\parallel} d\ell}{B\rho}$$

For a 5 Tesla-meters integrated solenoid field strength, the resulting spin resonance strength is about 0.02 at the injection energy and 0.003 at 250 GeV/c.

With longitudinal polarization at the collision point the longitudinal field rotates the polarization around its axis and thus changes the spin tune. The spin tune is changed by 0.03 to 0.003 at 25 GeV and 250 GeV, respectively, by a 5 Tm solenoid. This can be compensated by adjusting the direction of the axes around which the Snakes rotate the spin. By adjusting up to $\pm 5^{\circ}$ the spin tune can be adjusted for energies down to 25 GeV.

4.5. Helical Magnet Prototype

A prototype superconducting helical dipole magnet is being produced at BNL. The design of the $1\,m$ long, 180° twist helical magnet prototype follows the principles that are required in the operation of any superconducting magnet: that high forces be contained, that superconductor motion (particularly stick/slip motion) be minimized, that energy be safely extracted from the magnet at quench, that the ends of the magnet be restrained, that cooling be adequate for the operational conditions, etc. A number of concepts developed in the SSC and RHIC magnet programs are used, in particular the construction method used for the coils of the RHIC sextupole magnet. The construction of the spiral coil uses a new concept: grooves milled into a thick-walled aluminum cylinder to give a $cos(\theta)$ current distribution when the grooves are filled with conductor. In the initial models the coils are wound by hand. This can be done without a large tooling expense. In production some relatively straightforward tooling can be built to reduce the labor required to acceptable levels.

The superconductor wire developed in the RHIC corrector program is used by winding it into a 7-strand cable. This cable, nearly $1\,mm$ in diameter, requires $382\,A$ to produce a $4\,T$ field in the present design. By using this existing wire, the need to develop a new superconductor has been circumvented. Using a cable in the magnet is preferable to using a single wire: if a break in a wire should occur, the magnet would very likely still operate. In additional, a cable is more flexible than an equivalent wire to ease manufacturing of the coils. The required Kapton insulation is wrapped onto the cable in the manufacturing operation.

The cable is hand-wound under slight tension in an ordered pattern into Kapton-lined slots milled into an aluminum cylinder. A piece of prepreg fiberglass cloth is placed between each layer of wires in the slots. Pins at the ends allow the winding to proceed without wires bunching together. When all the turns have been wound onto the cylinder, each current block is compressed with ring clamps and then the entire assembly is placed into an oven for curing, thereby forming a series of current blocks around the cylinder in which each wire is firmly supported in a fiberglass/epoxy matrix. This design for supporting the cable turns is analogous to that developed for the wire turns in the RHIC sextupole magnet. The ends are filled with a mineral-loaded epoxy and cured in a follow-on operation, a technique used in the SSC program for adding strength and rigidity to coil ends.

Three of these cylinders, concentric with one another, are required to give the required field of 4 T. These three cylinders are mounted into an iron yoke supported one on the other with a slight clearance between finished cylinders. The finished size of each cylinder is achieved by overwrapping each cylinder with Kevlar strand to compress the current blocks and then with bands of fiberglass/epoxy, followed by grinding to size. A helium containment shell is welded in place around the yoke, serving also as the magnet support structure. From this point, the design is similar to that of the arc magnets for RHIC and all the same concepts and methods are used as appropriate.

It is estimated that the helical magnet operating at $4.2\,K$ will have a margin in field of 17 % above $4\,T$. This is a somewhat slender margin for an untested design such as this, so an operating field of $3.8\,T$ is recommended for this design, giving in that case a margin of 23 %. Undesired harmonics are easily minimized in this design by adjusting the thickness of the walls between current blocks, a procedure analogous to adjusting coil wedges in a conventional magnet.

Table 4.3 lists the design parameters of the prototype helical magnet and Table 4.4 shows the parameters of the superconducting cable used. Figure 17 shows a cross section of the coil structure. Figure 18 is an isometric view of the inner coil. Figure 19 shows a preliminary layout of the coils in the iron yoke; the dimensions of the yoke have not yet been optimized.

Operating Field	$4\,T$
Operating current	$382\,A$
Operating temperature	$4.2\,K$
Quench field @ $4.2\,K$	$4.67\,T$
Quench current @ $4.2\,K$	$453\,A$
Peak field at conductor at quench	$5.25\,T$
Inductance	$1.5\,H$
Stored Energy at operating field	$112\,kJ$
Total length incl. coil ends	$1.524\,m$
Helix length	$1.100\,m$
Helix Twist	$180°$
Helix Pitch	$0.1636°/mm$

Table 4.3: Parameters for the prototype helical magnet. The prototype represents half of a full twist helical magnet. The Siberian Snakes and the spin rotators are each constructed from four full twist helical magnets.

Wire:	Filament diameter	$10\,\mu m$
	Filament spacing	$> 1\mu m$
	Cu to non-Cu ratio	$(2.5 \pm 0.1) : 1$
	Number of filaments	310 ± 5
	Diameter, bare	$0.013 \pm 0.0001\,in$
	Minimum crit. current @ $5.0\,T, 4.2\,K$	$68\,A$
Cable:	Number of Wires	$7\,(6 - around - 1)$
	Diameter, bare	$0.039\,in$
	Diameter, insulated	$0.043\,in$
	Minimum crit. current @ $5.0\,T, 4.2\,K$	$476\,A$

Table 4.4: Parameters of the superconducting cable used for the prototype helical magnet.

5. Acceleration of Polarized Protons in RHIC

5.1. Depolarizing Resonance Strengths

Without Siberian Snakes there are numerous depolarizing resonances in RHIC, both intrinsic and imperfection resonances. The strengths of the intrinsic resonances can be calculated quite accurately from the appropriate integral over the horizontal focusing fields. Fig. 20 shows the result for the RHIC92 lattice with $\beta^* = 10\,m$ at all intersections. A calculation with $\beta^* = 1\,m$ gave only a slightly different result. The calculation was performed for a particle with a normalized Courant-Snyder invariant of $\varepsilon_0 = 10\,\pi\,mm\,mrad$. For a different value of the invariant the strength scales according to

$$\epsilon = \epsilon_0 \sqrt{\frac{\varepsilon}{\varepsilon_0}}$$

where ϵ_0 is the resonance strength for the invariant ε_0.

Important intrinsic spin resonances are located at

$$G\gamma = kP \pm \nu_y \approx mPM \pm \nu_B, \tag{5.1}$$

where k and m are integers, P is the superperiodicity of the accelerator, M is the number of FODO cells per superperiod, and $2\pi\nu_B = 2\pi(\nu_y - 6)$ is the accumulated phase advance of all FODO cells, which contain bending dipoles. The locations of the 3 strongest intrinsic resonances are

$$\begin{array}{rccc} G\gamma = & 3\times 81 + (\nu_y - 6), & 5\times 81 - (\nu_y - 6), & 5\times 81 + (\nu_y - 6) \\ E = & 139\,GeV, & 200\,GeV, & 224\,GeV \end{array}$$

where 81 is the product of superperiodicity, 3, and the "effective" FODO cells per superperiod, 27, which includes dispersion suppressors. The strengths of all 3 strong resonances are less than 0.5.

Important imperfection resonances are located at an integer closest to strong intrinsic resonances. This is clearly shown in the top part of Fig. 21 which shows the calculated imperfection resonance strengths for an uncorrected closed orbit obtained from a random sample of magnet misalignments with a rms spread of $\pm 0.5\,mm$, dipole roll angles with a spread of $\pm 1\,mrad$, dipole field errors of $\pm 5\times 10^{-4}$, and position monitor errors of $\pm 0.5\,mm$. After the closed orbit correction scheme MICADO was applied the strengths are greatly reduced as shown in the lower part for Fig. 21. The strengths of the imperfection resonances generally increase linearly with the beam energy and are bounded by

$$\epsilon_{imp} = 0.25\,\frac{\gamma}{250}\,\sigma_y$$

where σ_y is the rms value of the residual closed orbit excursions. The strength is smaller than 0.04 for all energies.

5.2. Effect of Siberian Snakes

With the installation of Siberian Snakes, which are local 180° spin rotators, the spin tune becomes 1/2, independent of the beam energy. Clearly the depolarizing resonance conditions cannot be met anymore as long as the fractional betatron tune $\Delta\nu_y \neq 1/2$ and therefore, in principle, no depolarization would occur. This is in fact true as long as the depolarizing resonances are not too strong. However, in the presence of strong resonances depolarization can occur from resonance conditions extended over more than just one turn. This leads to additional possible depolarizing resonance conditions:

$$\Delta\nu_y = \frac{\nu_{sp} \pm k}{n}$$

They are called Snake resonances[10] and n , the number of turns, is called the Snake resonance order. For two Snakes, as proposed here for RHIC, significant depolarization from Snake resonances only occurs for an intrinsic resonance strength of about 0.5 and even order Snake resonances require in addition an imperfection resonance strength of about 0.05. Fig. 22 shows the result of tracking through a region with an intrinsic resonance of strength 0.5 and

an imperfection resonance of strength 0.05. There are clearly regions of the betatron tune that do not experience any depolarization. Since the betatron tunes of RHIC were chosen to be located between 4/5 and 5/6, the betatron tune could be fit between the Snake resonances $13/16 = 0.8125$ and $5/6 = 0.8333$. With the betatron tune including its spread located between 0.815 and 0.830, a 0.015 range, no depolarization will occur over the whole RHIC energy range up to the top energy.

If the betatron tune spread is too large to fit into this range, some depolarization will be caused by the Snake resonance $\Delta\nu_y = 13/16$. Tracking calculations performed with an acceleration rate of $\dot{\gamma} = 3.9$ /sec showed that a gaussian beam with $\varepsilon_{N,95\%} = 20\pi\, mm\, mrad$ and with 10 % of the beam overlapping the 13/16 Snake resonance less than 5 % of the polarization is lost for each passage through one of the strong intrinsic resonances. The final polarization after passing all 3 strong resonances would then be at least 86 % of the injected polarization. It is important to note that, unlike for electron beams, the betatron tune distribution within the proton beam is basically static and does not get mixed. This means that depolarization experienced by a part of the beam is confined to this part only and will not affect the whole beam. In other words, there is no diffusion of polarization.

5.3. Sextupole Depolarizing Resonances

Spin resonances arising from sextupoles are located at

$$\nu_{sp} = kP \pm \nu_x \pm \nu_y = mPM \pm (\nu_x - 6) \pm (\nu_y - 6)$$

with resonance strength given by,

$$\epsilon_K \approx \frac{1+G\gamma}{8\pi}\sqrt{\frac{\varepsilon_x\varepsilon_y}{\pi^2}}\sqrt{\beta_x\beta_y}PM(|S_F| + |S_D|),$$

where S_F, S_D are respectively strengths of sextupoles located at the focusing and defocusing quadrupole locations. Because the emittance decreases with energy, the sextupole spin resonance strength is energy independent in hadron storage rings. For RHIC, the resonance strength is about 0.0003 at a normalized emittance of $20\pi\, mm\, mrad$. Such a sextupole driven resonance has been observed in the IUCF Cooler Ring. However , because of their small spin resonance strength, depolarizing resonances due to sextupoles are not important as long as the betatron tunes are chosen to avoid the resonance condition, which for a spin tune of 1/2 is

$$\frac{1}{2} = kP \pm \nu_x \pm \nu_y$$

The current working point for RHIC certainly avoids this condition.

5.4. Spin Tune Spread and Modulation

With snakes, the spin tune is independent of energy. Therefore the synchrotron motion does not give rise to spin tune spread. This has been verified indirectly in the snake experiment at the IUCF Cooler Ring, where one finds that there is no depolarization at the synchrotron side band for a 100% snake. However the spin tune modulation may still arise from imperfect spin rotation in the snake, and imperfect orbital angle between snakes. The errors in orbital angle may arise from survey error, closed orbit error, and/or betatron motion.

For an imperfection resonance strength $\epsilon = 0.05$ with two snakes, the perturbed spin tune shift is given by, $\Delta\nu_{sp} = \frac{\pi|\epsilon|^2}{4} = 0.002$. The error in the spin rotation angle of two snakes contributes also to the imperfection resonance strength. Assuming that the relative error of the integrated field strength of each snake dipole is 10^{-3}, the error in the spin rotation angle of a snake should be about $\sqrt{8} \times 180 \times 10^{-3} = 0.5°$, where we have assumed that a snake is constructed from 8 dipoles. The effect of 2 snakes in the accelerator will give a resonance strength of the order $\epsilon_{imp}^{eq} \approx 0.004$, which is smaller than the imperfection resonances due to closed orbit errors.

The error $\Delta\theta$ in the orbital angle between the two snakes can give rise to a spin tune shift of $\Delta\nu_{sp} = \frac{1}{\pi}G\gamma\Delta\theta$. Since the error in the orbital angle gives rise to spin tune shift and not a spin tune spread, one can compensate the effect by adjusting the spin rotation axes of the snakes. A survey error of about $\Delta\theta \approx 0.1\, mrad$ leads to a spin tune shift of 0.01 at the highest energy. For such a survey error, active compensation by adjusting the snake spin rotation axes is needed but is well within the tuning range of the Snake design.

The closed orbit can also cause orbital angle error between snakes. Let us assume that the maximum closed orbit is about $\hat{a} \approx 6\sigma \approx 1.0$ mm. The angular deviation is of the order of $\Delta x'_{co} \approx \frac{\hat{a}}{\sqrt{\beta\hat{\beta}}}$, where $\hat{a}$ is the maximum orbit error and $\sqrt{\beta\hat{\beta}} \approx \frac{R}{\nu}$ is the average betatron amplitude function. The expected error is about $\Delta x'_{co} \approx 2 \times 10^{-5}$ for RHIC, which gives rise to a spin tune shift of 0.002.

Similarly the betatron oscillation can cause orbital angle modulations. The spin tune modulation is given by

$$\Delta\nu_{s,\beta} \approx \frac{1}{\pi} G\gamma \sqrt{\frac{\epsilon}{\beta}} = \frac{1}{\pi} G \sqrt{\frac{\gamma\epsilon_N}{\beta}}$$

The resulting spin tune spread is about 0.007 for a beam with 20π mm-mrad normalized emittance at 250 GeV.

Combining all the possible sources, we expect that the total spin tune *spread* to be about 0.009 (imperfection resonance and betatron motion) and a correctable spin tune *shift* of 0.012 (Snake survey error and closed orbit error).

5.5. Betatron Tune Spreads and Modulations

In avoiding snake resonances up to the 13th order, the available tune space is about 0.015. With a spin tune spread of 0.009, the betatron tune needs to be controlled to better the 0.006. The tight requirements for the spin and betatron tune spread are only relevant while accelerating through the 3 strong intrinsic resonances when the beam-beam tune shift is negligible.

At the injection energy, the space charge tune spread can be as large as 0.02 for RHIC. However, the corresponding spin resonance strength at low energy is also about a factor of 3 smaller and therefore the available tune space is much larger.

6. Collision of Polarized Protons in RHIC

6.1. Polarization Lifetime

In storage mode even a very small depolarizing resonance strength can in principle lead to significant depolarization. This was observed at the ZGS where the effect of high order depolarizing resonances were studied on a 1 second flat top as shown in Fig. 23[16]. In an accelerator without Snakes like the ZGS the spin tune is energy dependent ($\nu_{sp} = G\gamma$) and therefore if the resonance condition is within the energy spread of the beam each proton will cross the resonance condition repeatedly and eventually the whole beam can be depolarized. With Snakes, however, the spin tune is energy independent and therefore all Snake resonance conditions are energy independent. As pointed out earlier and shown in Fig. 22 the beam can overlap higher order Snake resonances due to the betatron tune spread. Results of spin tracking calculations for a proton with $\Delta\nu_y = \frac{13}{16}$ and a Snake resonance strength of 0.15 showed that the spin vector is precessing about the vertical axis. At a resonance strength of 0.15, the vertical projection is about 90%. This precession is in fact a spin closed orbit in a broader sense of 16 turns. Spin tracking calculations were calculated over 8×10^9 turns without significant deviations from this spin closed orbit. Only a small fraction of particles are located within the width of the resonance and therefore effective depolarization in the storage mode is small.

When the spin vector is acted on with an adiabatic modulation within the tolerable limit, the spin vector will follow the spin closed orbit adiabatically. Non-adiabatic processes, arising from rf noise at the spin precession frequency, can indeed cause beam depolarization. Let us consider that a single dipole with strength θ_k is modulated at $\nu_{sp} f_0$, which is about 39 kHz for RHIC. The corresponding induced spin precessing kick is $G\gamma\theta_k$. The number of turns that occur before the spin is perturbed to 80% of the original polarization is given by,

$$N_p = \frac{\arccos[0.8]}{G\gamma\theta_k}$$

Let us now consider the same angular kick to the orbital motion. If there is an rf source at $\nu_{sp} f_0$, one expects a similar angular kick at the frequency qf_0, where q is the fractional part of the betatron tune. The orbital survival turn number is given by

$$N_o = \frac{A}{\langle\beta\rangle\theta_k}$$

where $\langle\beta\rangle$ is the average betatron amplitude, and A is the dynamic aperture. Using $A = 0.01$ m, $\langle\beta\rangle = 20$ m for RHIC, we find that the orbital lifetime is only half as long as the polarization lifetime.

Indeed, any rf source at high frequencies around the synchrotron and betatron tunes, are dangerous to the orbital stability of particles in accelerators. Similarly, any rf source at the spin tune can cause beam depolarization. These high frequency rf sources should be addressed carefully in hardware design.

6.2. Luminosity of Polarized Proton Collisions

The luminosity of RHIC is given by

$$\mathcal{L} = \frac{3 f_0 B N_B^2 \gamma}{2\epsilon_N \beta^*}$$

where f_0 is the revolution frequency, B is the number of bunches in each ring, N_B is the number of particles per bunch, ϵ_N is the normalized emittance, β^* is the amplitude function at the interaction point, and $\gamma = E/mc^2$. For a β^* of 2 m, 20π mm-mrad emittance, 57 bunches, and 10^{11} protons per bunch (nominal RHIC proton parameters), the luminosity at 250 GeV is 2.9×10^{31} cm^{-2}sec^{-1}. The above expression suggests a linear dependance of luminosity with beam energy. However, as the energy of the beam is decreased, the beam size in the interaction region triplet will increase. Hence, once a certain energy is reached (approximately 70 GeV in RHIC), the amplitude function at the interaction point must be optimized to maintain a maximum beam size in the low-beta triplet quadrupoles. With this scenario in mind, the luminosity at lower energies decreases more rapidly than linear.

The RHIC beam intensity can likely be raised to 2×10^{11} protons per bunch, and the interaction region optics is capable of generating a β^* of 1 m. In addition, the number of bunches can also be easily increased by a factor of two to 114. Thus the potential exists to produce a polarized proton luminosity at 250 GeV of 2×10^{32} cm^{-2} s^{-1}, which corresponds to one interaction per crossing for the $B = 114$ bunches per ring. Even higher luminosity might possibly be achieved with lower emittance, or with higher beam current. The luminosity for polarized protons vs. energy is shown in Fig. 24. For this figure, we assume an emittance of 20π mm-mr emittance, 2×10^{11} protons per bunch, and β^* at high energy of 1 m. At 25 GeV, $\beta^* = 2.8$ m in order to maintain the required beam size in the triplet quadrupoles.

7. Measuring the Beam Polarization in RHIC

7.1. Polarimeter Lay-out

We propose to construct two polarimeters that are capable of measuring the polarization of the circulating beam in each ring independently at various stages in the acceleration cycles.

These polarimeters utilize the asymmetries (A_n) in inclusive pion production at high X that were measured at the Argonne ZGS [17] and at Fermilab[18]. The asymmetries increase linearly with X and appear to be independent of the incident polarized beam momentum. Moreover, the ZGS data which were taken with both liquid hydrogen and deuterium targets show no dependence on target nuclei. Since these polarimeters will use a fixed target, the ZGS and Fermilab measurements cover the full energy range of the RHIC beams. We would like to measure the pion asymmetry at the desired kinematic region at the AGS to obtain directly the analyzing power at the RHIC injection energy, and to verify the apparent energy independence of the analyzing power.

The polarimeters are designed to probe the kinematic region of 0.5 in X and $0.8\,GeV/c$ in transverse momentum of the scattered pions. This was optimized from the Fermilab data based on the fact that the asymmetry rises linearly with X while the cross section is falling as $(1-X)^2$, and that the error in the asymmetry measurement is the inverse of the square root of the total number of events.

We propose to use π^- asymmetry, since π^- are a relatively large fraction of negatives, and particle identification is therefore not necessary. At the chosen parameters, the measured π^- asymmetry is 14% and the invariant cross section is about $100\,\frac{\mu b}{GeV^2}$[19].

The polarimeters are designed to fit in the 40 meter long straight sections between Q3 and Q4. The apparatus consists of a $5\,\mu m$ carbon fiber target, followed by a 2 meter long dipole magnet with a $1\,GeV/c$ transverse momentum kick, and then a hadron calorimeter. The scattering angle and selected spectrometer momentum depend on the beam energy: at RHIC injection of $25\,GeV/c$, the scattering angle would be $64\,mrad$ and the π^- momentum $12.5\,GeV/c$; at $250\,GeV/c$ RHIC beam momentum, the scattering angle is $6.4\,mrad$ and the π^- momentum is $125\,GeV/c$. For the smallest angle, 6.4 mrad, the spectrometer magnet will be 30 meters from the target, giving a 20 cm. displacement from the beam center. The magnet aperture will be 2 cm.(H) x 6 cm.(V), and the small angle position constrains the magnet septum width. The detector system will extend 10 meters downstream from the magnet. The magnet kick and the positioning of the downstream detection elements will minimize the contamination from straight through neutrals. Upstream of this magnet we envisage using collimation to cut down on background. The detection apparatus will consist of several trigger counters followed by a hadron calorimeter with energy resolution $\frac{\Delta E}{E} = 40\,\%/\sqrt{E}$, with E in GeV. This provides an 11% measurement at $12.5\,GeV/c$. The whole assembly will rotate in order to accommodate the changes in the scattered angle as the circulating beam energy increases. In addition, we require that the magnet and detector move upstream for the lower energy, wide-angle measurements. An increased acceptance is necessary at lower energy: the emittance blow-up from multiple-scattering in the fiber target over the measuring time must be kept to within acceptable limits. The table below uses a 9.5 meter position for the magnet for the 25 GeV measurements. We also envision that the assembly will translate together with the fiber target when the target is moved into the beam, maintaining a fixed geometry independent of the transverse position of the target.

We use a $5\,\mu m$ carbon fiber target, a π^- momentum bite of 0.1, X = .5, and p_T = 0.8 GeV/c in the following table. 10^4 π^- are collected to obtain a 7% error in polarization. The emittance increase from multiple scattering is proportional to the lattice β function at the fiber target, so we must place the target near Q4 in the RHIC lattice and scatter toward the intersection region, giving $\beta = 25$ meters at the fiber target. (The polarimeter measurements are for short periods, and the experiment at that intersection region would be gated off for these periods.) We obtain the following table:

	25 GeV	**250 GeV**
$\Delta\Omega$	$13\,\mu sr$	$1.3\,\mu sr$
$\Delta\epsilon_N$	$7\,\pi\,mm\,mrad$	$0.07\,\pi\,mm\,mrad$
interacting beam fraction:	3×10^{-3}	3×10^{-4}
measuring time:	$1\,s$	$0.03\,s$

These calculations are for 57 bunches and 10^{11} protons/bunch. The emittance growth at 25 GeV is about 20%

for the measurement. Thus, the measurements at 25 GeV would be considered destructive. Measurements at 250 GeV can be parasitic. Beam loss from nuclear interactions is quite small–about 0.2% for the 25 GeV measurements. As can be seen from the table, measurement time is quite short. The target thickness, acceptance, and number of bunches used (for example, for commissioning) will be optimized, since these choices depend on the number of stored protons, rates in the detector, and the desired polarization error.

7.2. Heating of the Carbon Fiber

To minimize the contribution of multiple scattering to the emittance growth, the polarimeter fiber is located close to Q4. The betatron functions in x and y are small and similar at this location [RHIC Conceptual Design Rep., p.74]

$$\beta_{x,y} \simeq 25\,m$$

We then obtain the rms beam size for the worst case, 250 GeV/c,

$$\sigma = \sqrt{\frac{\beta\epsilon_N}{6\pi\gamma}} = 0.57\,mm$$

Since $\sigma \gg d_{fiber}$ the irradiation of the fiber is essentially uniform (i.e. there isn't any "hot spot" at the beam core).

The incident power per bunch is

$$P_i = 0.3 N_{bunch} f_{rev.} \frac{dE}{dx} d_{fiber}.$$

The factor 0.3 is from CERN studies of wires in beam.

$$\begin{aligned} P_i &= 0.3 \times 10^{11} \times 80\,kHz \times 2\frac{MeV cm^2}{g} \times 2.3\frac{g}{cm^3} \times 5 \times 10^{-4}\,cm \times 1.6x10^{-13}\frac{J}{MeV} \times 0.006\sqrt{\frac{P_{beam}}{250\,GeV}} \\ &= 5.4\frac{mJ}{s} \end{aligned}$$

This was calculated for a 5 micrometer fiber. The factor $0.006\sqrt{\frac{P_{beam}}{250\,GeV}}$ is the ratio of beam area that the fiber intercepts. The radiated power is

$$P_r = \sigma_B \varepsilon A T^4.$$

For carbon, $\varepsilon = 0.9$, $A = (4d_{fiber}) \times 2\sigma_{beam}$ (for a square fiber), $P_r = 12 \times 10^{-16} T^4$, for 250 GeV beam. The equilibrium temperature for 52 bunches is

$$\begin{aligned} P_r(T_{equilibrium}) &= 52 P_i \\ T_{equilibrium} &= 3900^\circ K \text{ or } 3627^\circ C. \end{aligned}$$

The sublimation temperature for carbon is $3500^\circ C$, so this is too hot. We may choose to use a smaller fiber or insert the fiber for only a short time. A $1\,\mu m$ fiber would reduce the incident power by a factor of 25, and the temperature by a factor 2.2.

7.3. Detector Remarks

We have not yet decided on the π^- detector or the final geometry. A study of tracking showed that a device such as a gas or silicon microstrip detector with 5 horizontal measuring planes arranged around the magnet, $0.1\,mm$ pitch or spacing, would reconstruct the π^- tracks with only 2% of the tracks incorrectly reconstructed. The average number of hits in the front plane was 20 for one bunch crossing.

We have been using a magnet kick of $1\,GeV/c$, but this would be insufficient to provide room for the transverse dimensions of typical calorimeters. Usually 1 interaction length is required transverse to the shower. If a ZEUS-type hadronic calorimeter is used, which would have the energy resolution we have assumed above, the half-width of the calorimeter is $40\,cm$. We would only have space for about $20\,cm$, and we would also have to shield the calorimeter from neutral and positively charged particles.

Therefore, we may prefer either a scintillator detector or tracking.

Another issue which has not been resolved is whether two arms (left and right) might be necessary. The geometry of the Q3-Q4 region, where the two stored beams are separated by only 20 cm, precludes a 2-arm polarimeter with our indicated design. One experience with low-energy polarimeters, which are based on elastic scattering, is that averaging left and right polarimeter measurements has been necessary for the stability of the result. We must evaluate the difference between the two types of polarimeters to judge the importance of two vs. one arm for the RHIC polarimeter.

8. Spin Reversal of the Stored Beams

Since the proposed asymmetry measurements are high precision measurements, frequent polarization sign reversal is imperative to avoid systematic errors. Possible sources for systematic errors are luminosity variations, crossing angle variations, and detector efficiency variations. As mentioned earlier different bunches will have different polarization sign and therefore different bunch crossings will measure interactions with different combinations of incoming beam polarization signs. Although this will greatly reduce systematic errors it is still true that one pair of bunches would always cross with the same combination of polarization signs during the whole lifetime of the stored beams which is at least several hours. To eliminate the possibility of systematic errors from this situation we propose to install a spin flipper in each ring which is capable of reversing the polarization sign of all bunches. A spin flipper typically consists of horizontal DC dipole magnets interleaved with laminated vertical dipole magnets[12]. Exciting the vertical magnets with about $40\,kHz$ AC current would drive an artificial spin resonance which can be used to adiabatically reverse the polarization direction. Fig. 25 shows the result of a test of this concept performed at the Indiana University Cyclotron Facility (IUCF)[15].We estimate that complete spin reversal would take less than 1 second. The same device will be used to accurately measure the spin tune by measuring the spin reversal efficiency as a function of the frequency of the spin flipper excitation. This is instrumental to adjust the spin tune to 0.500.

In most cases a simple oscillating driving field is very effective in driving an artificial resonance since the oscillating field can be thought of as the sum of two counter-rotating fields, only one of which is in resonance with the beam precession frequency. However, with a Snake the spin tune is a half-integer and therefore the two counter-rotating fields are both in resonance and interfere so that effectively only half of the beam around the ring circumference sees a driving field. By designing a true rotating field the beam polarization can be fully flipped even with a half-integer spin tune.

Several designs have been proposed, all involving two sets on AC magnets with a 90° phase difference between them. The first design uses three strong DC magnets interleaved with four independently driven vertical AC magnets. Table 8.1 shows the parameters of such a spin flipper, which could fit into a regular $12\,m$ straight section. The DC magnets in this first design are quite strong and expensive. A less expensive design would utilize one of the two Siberian Snakes instead of special DC magnets. The two sets of vertical AC magnets are placed symmetrically around the Snake with one set generating a vertical bump of half a vertical betatron wavelength and the other one a full wavelength long. By driving the bumps with $40\,kHz$ AC 90° out of phase a rotating driving field will be generated. Figure 26 shows a schematic layout for the magnet arrangement for such a spin flipper. To achieve full spin flip with less than .01 % polarization loss per flip a field integral per AC magnet of $\int Bdl = 0.01\,Tm$ and a flip time of about $1.0\,s$ is required[13].

Since the orbit might not be completely corrected by the spin flipper magnets, emittance blow-up could result the residual beam deflection. The total deflection in the vertical magnets is about $100\,\mu rad$ at $25\,GeV$ and correspondingly less at higher energies. The residual deflection can then be less than $\Delta y' = 1\,\mu rad$. The betatron amplitude after n turns is then

Magnet	Strength	Excitation
1.Vertical magnet	$0.01\,Tm$	$\sin\omega t$
2.Horizontal magnet	$+4.2\,Tm$	DC
3.Vertical magnet	$0.01\,Tm$	$-2\sin\omega t + \cos\omega t$
4.Horizontal magnet	$-8.4\,Tm$	DC
5.Vertical magnet	$0.01\,Tm$	$\sin\omega t - 2\cos\omega t$
6.Horizontal magnet	$+4.2\,Tm$	DC
7.Vertical magnet	$0.01\,Tm$	$\cos\omega t$

Table 8.1: Parameters for a spin flipper that produces a true rotating driving field. The excitation of the AC magnets indicates the relative phase shift between the four magnets.

$$\begin{aligned} y &= \beta \Delta y' \sum_{m=1}^{n} \cos(2\pi\nu_{sp} m) \sin(2\pi\nu_y (n-m)) \\ &= \tfrac{1}{2}\beta \Delta y' \left[\cos(2\pi\nu_y n) - \sin(2\pi\nu_y) \tfrac{\cos(2\pi\nu_{sp} n) - \cos(2\pi\nu_y n)}{\cos(2\pi\nu_{sp}) - \cos(2\pi\nu_y)} \right] \end{aligned}$$

with a maximum value of $0.024\,mm$ for $\nu_{sp} = 0.5$ and $\nu_y = 0.8$. This results in a contribution of $6 \times 10^{-4}\,\pi\,mm\,mrad$ to the normalized emittance of the beam. The above formula is only valid if the coherence of the kicked beam is maintained. In reality the motion will decohere but not faster than within about 100 turns, corresponding to a tune spread of less than 0.01. As a result the emittance will increase linearly during the time the spin flipper is on. However, the emittance increase is less than

$$\frac{1.0\,s \times f_{rev}}{100} \times 6 \times 10^{-4}\,\pi\,mm\,mrad = 0.5\,\pi\,mm\,mrad$$

which is negligible compared to the $20\,\pi\,mm\,mrad$ beam emittance.

9. Commissioning and Physics–Issues and Approach

Our goal is to collide 70 % polarized protons beams in RHIC with luminosity up to $2 \times 10^{32} cm^{-2} sec^{-1}$. A_{LL}, A_L, A_{NN}, and A_N are to be measured at STAR and PHENIX, and A_{NN} and A_N at one or more other intersections. The statistical errors can be quite small–for example, 10^{-3} in asymmetry for jets with $p_T > 40 GeV/c$ is desirable and achievable. Physics measurements will explore a wide energy range: $\sqrt{s} = 50$ to $500\, GeV$.

In this section we outline an approach to commissioning the polarized proton collider and we discuss several issues for physics running.

9.1. Operational Modes of RHIC for Polarized Proton Running

For normal operation no special operational modes of RHIC are required for the acceleration and storage of polarized protons. Since depolarizing resonances are driven predominantly by vertical orbit excursions, particular care has to be given to the corrected vertical closed orbit and the vertical beam emittance. This means that beam blow-up from beam-beam interactions and stop-bands should be minimized. To avoid depolarization from snake resonances the fractional vertical betatron tune including tune spread has to be kept well within $\frac{13}{16} = 0.8125$ and $\frac{5}{6} = 0.8333$, especially at the energies of the 3 strongest intrinsic resonances: $G\gamma = 3 \times 81 + (\nu_y - 6)[E = 139 GeV]$, $5 \times 81 - (\nu_y - 6)[E = 200 GeV]$, $5 \times 81 + (\nu_y - 6)[E = 224 GeV]$. Also the acceleration rate would have to be at least $\dot{\gamma} = 4.2\, s^{-1}$, which corresponds to $\frac{dB}{dt} = 0.05\, T/s$.

During commissioning, acceleration cycles that allow for polarization measurements at various energies are required, in particular at the injection energy, at energies below and above the 3 strongest intrinsic resonances, and at some intermediate energies: $25\, GeV$, $50\, GeV$, $100\, GeV$.

9.2. Commissioning

9.2.1. Considerations

The commissioning approach will be step-wise, beginning with one ring, no polarization, and advancing to both rings polarized at full energy. We assume here that, at the time that RHIC begins polarized proton studies, RHIC will have already been fully commissioned for protons and heavy ions, and the AGS will be a well-understood injector for polarized protons. (E880, the partial snake experiment in the AGS, will have been completed.)

It is important for efficient commissioning to optimize the measurement cycle, filling → polarization measurement → filling, and on-line polarization results are required. With an inclusive π^- polarimeter in each ring, we estimate that this cycle can be kept to about 5 minutes, with a 5 % polarization measurement from each cycle. We position the polarimeter for maximum acceptance at the desired kinematic region ($X = 0.5, p_T = 0.8 GeV/c$). The polarimeter target thickness and number of bunches in the ring can be chosen to optimize the turn-around, depending on the number of protons stored, and the acceptable singles rate in the polarimeter. For the example used in the polarimeter section, we used a $20 \mu sr$ acceptance for $25 GeV/c$ beam, 10^{11} protons per bunch, 57 bunches filling one ring, and a 5 micron carbon fiber target. This gave a 5 % polarization measurement in 1 second, with an emittance blow-up from multiple scattering in the target of $\Delta\, \varepsilon_N = 4\pi\, mm\, mrad$. For commissioning it would be acceptable to have the emittance increase by 10π (50 % of the initial emittance of 20π). It may be desirable to fill the ring with a smaller number of bunches if that reduces the cycle time. We assume that half the bunches would be loaded with spin up and half with spin down, for each cycle. Scalers would count the inclusive π^- seen by the polarimeter, gated for the spin direction. Polarization is obtained on-line from

$$P = \frac{1}{.18} \frac{N(up) - N(down)}{N(up) + N(down)}$$

Besides the polarimeters, each ring will have an rf spin-flipper, described in section 8. This device can be used to measure the spin tune. At the resonant frequency of the device, the polarization can be adiabatically reversed. If left on for a longer time, the polarization will be driven to zero. In this way, the resonant frequency can be identified:

by measuring the polarization at different frequencies. The spin tune is then the resonant frequency divided by the revolution frequency:

$$\nu_{sp} = \frac{f_{rf,res.}}{f_{rev}}.$$

The spin tune can be measured very accurately, and the tune should be 0.500 if the Siberian Snakes are set up properly.

9.2.2. Commissioning Steps–One Ring only

A. Snakes off, establish bunched beam at 25 GeV to 250 GeV–closed orbit corrections, etc.

B. Turn on 1 snake, no polarization, 25 GeV

- adjust V, H, trim supplies for snake to center beam (use pick up electrodes–PUEs)
- adjust tune to correct for snake tune shift (use tune-meter)
- adjust multipole correction magnets for sufficient storage time (>5 minutes) (use current transformer)
- snake coupling correction with skew quads (use tune-meter– kick in one plane, measure tune in the other plane)
- measure orbit excursion inside snake (this requires a PUE at the center of the snake)

C. Turn on 2nd snake in ring (alone), and repeat b

- balance orbit excursion in both snakes

D. Both snakes on–check excursions and lifetime (don't anticipate a problem)

E. Polarimeter check-out

- target in/out, accidentals (assume calorimeter has been calibrated in a test beam)

F. Transverse polarization in one ring, 25 GeV, both snakes on (note that the snakes are not necessary to maintain polarization at 25 GeV)

- commission polarimeter–look for asymmetry
- no asymmetry? Check AGS polarization. If OK, vary transfer line.
- observe asymmetry. Check repeatability; put in $P = 0$, measure $P = 0$; turn off both snakes, should measure $P = P_{AGS}$; turn off one snake, should measure $P_y = 0$; small scan of (X, p_T) vs. NA^2 to optimize and check polarimeter.
- measure spin tune with rf spin flipper
- measure spin tune vs. energy–constant, 1/2 if the snake settings are correct. Otherwise, there are several possible effects. If the spin tune depends on energy, then the snakes would not be exactly 180 degrees apart in ring field integral. This is not expected (and is not correctable). If the spin tune is independent of energy but not 1/2, two effects can contribute: the snake axes are not orthogonal, or the snake precession angles are not 180 degrees. These can be explored and corrected by adjusting each separately.
- commission spin flipper
- at resonant rf frequency, measure polarization vs. time on to establish spin flip
- many spin flips–measure polarization loss from spin flipper

G. Accelerate–steps determined by spin resonances (measure just before, after expected resonance). Larger resonances at about 120, 140, 220, 240 GeV.

- need to check spin tune at lower energies (expect different effective lengths of snake magnets vs. orbit excursion)
- if the polarization is reduced or lost, measure spin tune and adjust snakes

- also measure asymmetry in polarimeter at the energy where the π^- asymmetry was measured at FNAL. This would give an absolute polarization for the beam which doesn't rely on the apparent energy independence between the ZGS and FNAL data.

H. Commission the spin rotators

- use polarimeters and measure the predicted P_y at the polarimeter position vs. different excitations of each rotator, and vs. energy
- if necessary, measure the absence of transverse polarization at the collision region
- the 1st approach is fine for A_{LL} and "large" A_L (W and Z) physics. Sensitive A_L searches are another matter.

I. Repeat for the 2nd ring

J. 2 rings–relative luminosity measurement and polarization lifetime (should be fine)

9.3. Physics Running–Issues

9.3.1. Bunch pattern

Each bunch can be filled independently, so the "pattern" of polarization direction for the 57 bunch positions in each ring can be arranged in an optimal way. At each intersection region the same pairs of bunches interact, but there are different pairs at each intersection. It is typically desirable to collide equal numbers of $(++, +-, -+, --)$ bunches at each experiment, where $+-$ represents a bunch in one beam with polarization up colliding with a bunch in the other beam with polarization down.

One solution which would satisfy all the intersections is to have one missing bunch in each ring, and load the 56 bunches of one ring $(+ + - - + + - - + + --$, etc.), and load the 56 bunches of the other ring with $(+ - + - + - + - + - +-$, etc.). The pattern and time of one bunch is given by RHIC to the experimenters. Each experiment chooses 52 collisions, ignoring 3 collisions, to have complete sets of $(++, +-, -+, --)$. This is illustrated in Figure 15.

9.3.2. Frequency of Spin Flip

Because the same bunches collide for a given experiment, periodically reversing the spin will reduce systematic errors for asymmetry measurements even further. Polarization reversal will take about 1 second. The frequency of reversal depends on the effect on luminosity from emittance blow-up, and on polarization loss from the flipping process. Neither is expected to be large.

9.3.3. Systematic Errors

Therefore, for each fill, the spin condition changes at each experiment every 220 nanoseconds or 1.6×10^{10} times per hour. In addition, the spin can be reversed for each crossing, possibly once per hour. Finally, the pattern can be changed for each fill.

Experiments making particularly sensitive asymmetry measurements may desire to measure relative luminosity of individual bunch crossings. An asymmetry measurement to 10^{-3} requires that the overall relative luminosity be known (or be equal) to 10^{-4}. If the individual bunch crossing luminosities are independent of spin state *or* the spin flip process is independent of spin state, then the luminosities will be equal. If this is not assumed, the experiment can measure the bunch crossing relative luminosity to 10^{-4} with a factor of 100 more counts in a luminosity monitor than signal. If the signal counts are 10^6, collected over 10^6 seconds, the luminosity monitor must have a rate $> 100\,Hz$.

9.3.4. Beam Polarization Measurements

The polarization measurements are unobtrusive at 250 GeV, with $< 1\,\%$ emittance growth to obtain a $5\,\%$ polarization measurement, in less than a second. At 25 GeV, the emittance growth becomes a problem, but this is not a typical running energy. The frequency of measurement depends on the stability of the system. We assume that a measurement would be made every hour, and the data for the previous hour would be thrown out if the polarization were lost.

10. Figure Captions

1. Layout of the AGS-RHIC accelerator complex showing all the major component that are necessary for the acceleration of polarized proton beams to the RHIC top energy.

2. View of RHIC overemphasizing the interaction regions to show the location of the Siberian Snakes and the spin rotators placed around the collider experiments STAR and PHENIX. Also shown are the polarization directions around the rings and around the detectors for collisions with longitudinal polarization.

3. The upper figure shows the measured vertical polarization as a function of spin tune $G\gamma$ for a 10 % Snake (solid dots) and without the Snake (open circles). Note that partial depolarization at $G\gamma = 8$ is avoided by using the 10 % Snake. The lower figure shows the absolute value of the vertical polarization at $G\gamma = n + \frac{1}{2}$ up to $G\gamma = 22.5$ (solid dots). Note that partial depolarization only occurs due to the intrinsic resonances.

4. The absolute value of the vertical polarization is shown as a function of energy for the April 1994 run (open circles) and the December 1994 run (solid dots). Note that during the December run most intrinsic resonances were successfully crossed with significant depolarization only at the intrinsic resonances $G\gamma = 0 + \nu_y, 12 + \nu_y, 36 + \nu_y$.

5. General layout of beam transport system between AGS and RHIC

6. Schematic diagram of the 20° bend of the ATR line. (Bending magnets only)

7. Schematic Diagram of the RHIC Injection Section

8. Directional cosines of the proton spin vector, as a function of at the entrance of the switching magnet for a central trajectory particle.

9. Directional cosines of the proton spin vector, as a function of at the RHIC injection point for a central trajectory particle.

10. Directional cosines of the proton spin vector, as a function of at the RHIC injection point for a non-central trajectory particle.

11. Schematic diagram of the three proposed dipoles showing their relative position with respect to the send vertically bending dipole.

12. Directional cosines of the proton spin vector, as a function of at the RHIC injection point for central trajectory particles. The first of the three dipole magnets (see text) has been tuned to maximize proton polarization at the entrance of the switching magnet for beam proton energy corresponding to $\gamma = 25$. The other two dipole restore the central trajectory and cancel the achromaticity introduced by the first dipole.

13. Orbit, field and spin tracking through the four helical magnets Siberian snake at $\gamma = 27$. The spin tracking shows the reversal of the vertical polarization.

14. Change of the direction of the snake rotation axis as a function of the excitation .

15. Orbit, field and spin tracking through the four helical magnets spin rotator at $\gamma = 27$. In this example, the spin tracking shows how the polarization is brought from vertical to horizontal.

16. Excitation of the two pairs of helical magnets in the rotator to achieve longitudinal polarization in the insertion of RHIC, for various beam energies.

17. Cross section of the coil structure of the prototype helical magnet.

18. Isometric view of the inner coil layer of the prototype helical magnet.

19. Preliminary layout of the three coil layers in the iron yoke of the prototype helical magnet.

20. Strengths of the intrinsic depolarizing resonances in RHIC calculated for the RHIC92 lattice and for both $\beta^* = 10\,m$ and $\beta^* = 1\,m$ at all six intersection points. There is no noticeable difference of the calculated strengths for the two values of β^*.

21. Strengths of the imperfection depolarizing resonances in RHIC calculated after simulating the MICADO orbit correction scheme.

22. Vertical component of the polarization after acceleration through a strong intrinsic resonance and a moderate imperfection resonance shown as a function of the fractual vertical betatron tune.

23. Depolarization on the 1 second flat top at the ZGS.

24. Polarized proton luminosity as a function of energy in RHIC. A normalized emittance of 20π mm-mr (95%), 114 bunches per ring, and a beam intensity of 2×10^{11} protons per bunch were used. A value of $\beta^* = 1$ m from 74 GeV to 250 GeV was assumed; at 25 GeV, β^* is 2.8 m.

25. Adiabatic spin reversal of a stored beam of polarized protons at the IUCF Cooler ring. The RF voltage is proportional to the strength of the artificial spin resonance driving the spin reversal.

26. Schematic diagram of spin-flipper with radio-frequency dipoles and a Siberian Snake

A. Cost Estimate and Schedule

A rough draft cost estimate and preliminary schedule for the project are shown in Tables A.1 and A.2. The cost of magnetic components are based upon the cost of RHIC 10 cm bore dipole magnets, scaled by length and complexity of the snakes and rotators as described in the text of this report. The costs presented are in FY95 dollars and the schedule is shown beginning on April 1, 1995. This start date is contingent upon arrival of proper funding on that date. The total cost of the project, including contingency, is approximately $10M, spread out over 4 years.

	Total K$
Snakes (4) and Rotators (8)	3658
Spin Flip Magnets (12)	479
Magnet Electrical Systems	930
Instrumentation (Polarimetry, BPMs, etc.)	478
Cryo, Vaccum, etc.	100
Controls and Software	190
Injector Modifications	400
Installation	483
EDIA	1781
Subtotal	8499
Contingency (25%)	1700
Total	10199

Table A.1: Summary of project cost estimate.

Table A.2: Project schedule (see following two pages)

	95				96				97				98				99			
	1	4	7	10	1	4	7	10	1	4	7	10	1	4	7	10	1	4	7	10
WORK to be PERFORMED (x = Now)	x																			
Magnet Systems																				
Snake Modules(2x2x4=16)																				
Prototypes		x	x	x	x															
16 Modules (4 snakes)					x	x	x	x	x	x	x	x	x							
Magnet measurements											x	x	x	x						
Rotator Modules(2x2x2x4=32)																				
Prototypes		x	x	x	x															
32 Modules (8 rotators)					x	x	x	x	x	x	x	x	x							
Magnet measurements											x	x	x	x						
Spin Flipper Modules(2x(3+3)=12)																				
Prototypes					x	x	x	x												
6 DC Magnets									x	x	x	x	x	x	x					
6 AC Magnets												x	x	x	x					
Magnet measurements														x	x					
Magnet Systems Interface																				
Magnet Electrical System																				
50 snake/rotator supplies										x	x	x	x							
6 spin flip DC supplies											x	x	x							
6 spin flip AC supplies											x	x	x							
quench protection							x	x	x	x										
System interface							x	x	x	x	x	x	x							
Cryogenics																				
System interface									x	x	x	x								
Vacuum																				
System interface									x	x	x	x								
Instrumentation																				
--Polarimeters																				
2 Polarimeter wire chambers						x	x	x	x	x	x	x	x	x	x					
2 Polarimeter detectors									x	x	x	x	x	x	x					
2 spectrometer magnets									x	x	x	x								
2 spectrometer magnet DC supplies											x	x	x							
System interface											x	x	x	x						
--BPMs, Loss monitors																				
12 BPMs						x	x	x	x											
24 Loss monitors									x	x	x	x								
System interface											x	x	x	x						
Controls																				
Crates and controllers, etc.							x	x	x	x										
Software procurement										x	x	x	x							
Conventional Facilities																				
modifications to RHIC facilities					x	x	x	x												

	95				96				97				98				99			
	1	4	7	10	1	4	7	10	1	4	7	10	1	4	7	10	1	4	7	10
Injector (AGS) Modifications																				
Magnetic Element/Systems				x	x	x	x	x	x											
Instrumentation/Systems				x	x	x	x	x	x											
Installation													x	x						
Commissioning														x	x	x				
Accelerator tests/experiments																				
helical snake prototype (?)					x	x														
single particle effects (?) at IUCF?				x				x				x								
tests of polarimetry apparatus (AGS)										x	x									
AGS runs -- meet RHIC Requirements				x				x				x				x				
System Installation																				
magnet stands												x	x	x	x					
cables														x	x	x	x			
survey/alignment																	x			
Labor Estimate (FTE/quarter)																				
Project Management		2	2	2	2	2	2	2	2	2	2	2	2	2	2	2	2			
Accelerator Physicists		2	2	2	2	2	2	2	2	2	2	2	2	2	2	2	2			
Magnet Division Physicists		1	1	1	1	1	1	1	1	1	1	1	1	1	1					
Magnet Division Engineers		1	1	1	1	1	1	1	1	1	1	1	1							
Magnet Division Designers		3	3	3	3	2	2	2	2											
Magnet Division Technicians		2	2	2	2	4	4	4	4	4	4	4	4	2	2					
Accelerator Engineers		0.5	0.5	0.5	0.5	0.5	1	1	1	2	2	2	2	3	3	3	3			
Accelerator Technicians										3	3	3	3	5	5	5	5			
Computer Programmers											0.5	0.5	0.5	0.5	1	1	1			
totals:		11.5	11.5	11.5	11.5	12.5	13	13	13	15	15.5	15.5	15.5	15.5	16	13	13			

BIBLIOGRAPHY

[1] Proposal on Spin Physics Using the RHIC Polarized Collider (R5), submitted to the BNL PAC October 1992

[2] J.G. Alessi et al., AIP Conf. Proc. No. 187, p. 1221 (1988)

[3] F.Z.Khiari et al., Phys. Rev. D39, 45 (1989)

[4] T.Roser, AIP Conf. Proc. No. 187, p.1442 (1988)

[5] H.Huang et al., Phys. Rev. Lett. 73, 2982 (1994)

[6] S.Y.Lee and E.D.Courant, BNL Technical Note AD/RHIC-63

[7] J.Claus and H.Foelsche, Beam Transfer from AGS to RHIC, RHIC 47, 1988

[8] V.I.Ptitsin and Yu.M.Shatunov, Helical Spin Rotators and Snakes, Proc. Third Workshop on Siberian Snakes and Spin Rotators (A.Luccio and Th.Roser Eds.) Upton, NY, Sept. 12-13,1994, Brookhaven National Laboratory Report BNL-52453, p.15

[9] A.Luccio, Program SNIG, unpublished, and SNIG Formalism Proc. Third Workshop on Siberian Snakes, loc. cit., p. 193.

[10] S.Y.Lee and S.Tepikian, Phys. Rev. Lett. 56, 1635 (1986)

[11] S.Y.Lee, Nucl. Inst. Methods, A306, 1 (1991)

[12] T.Roser, Spin Rotators and Split Siberian Snakes, NIM A342 (1994) 343.

[13] R.A.Phelps,Spin Flipping a Stored Polarized Proton Beam in the Presence of Siberian Snakes, Third Workshop on Siberian Snakes, loc. cit., p. 225.

[14] A. Luccio and M. Conte, Wiggler as Spin Rotators for RHIC, contribution to 1993 Particle Accelerator Conf., Washington, D.C.; E.A. Perevedentsev, V.I. Ptitsin and Yu.M. Shatunov, Spin Behavior in Helical Undulators, to be published.

[15] V.A.Anferov et al., IUCF Newsletter No. 50, p. 11 (1992)

[16] L.Ratner, private communication.

[17] Dragoset et al., Phys. Rev. D 18, 3939 (1976)

[18] D.L.Adams et al., Phys. Lett. B264, 462 (1991)

[19] L.G. Ratner et al., Proc. of the Rochester Meeting APS/DPF, Rochester, p. 99 (1971)

Polarized Proton Collisions at BNL

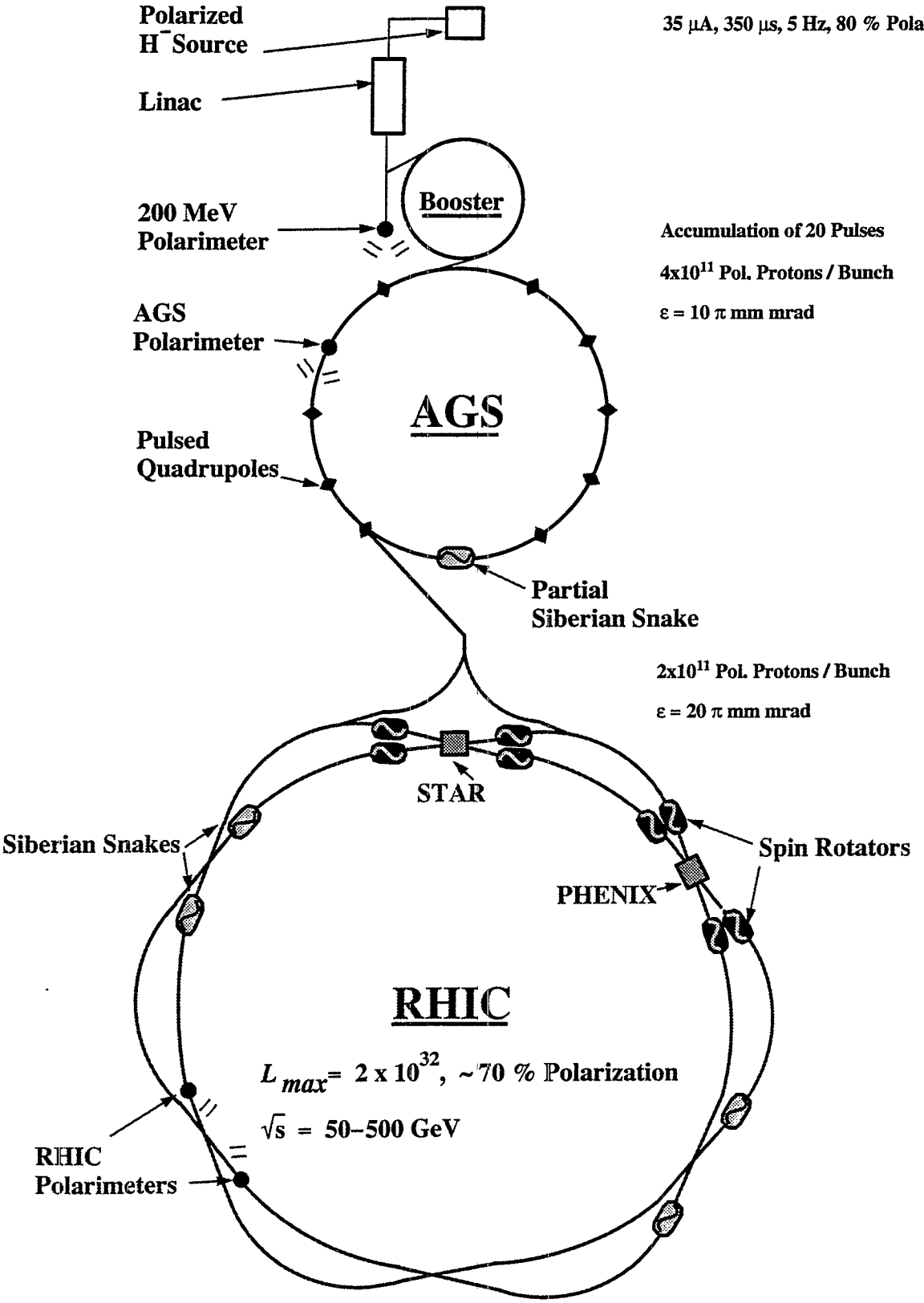

Figure 1

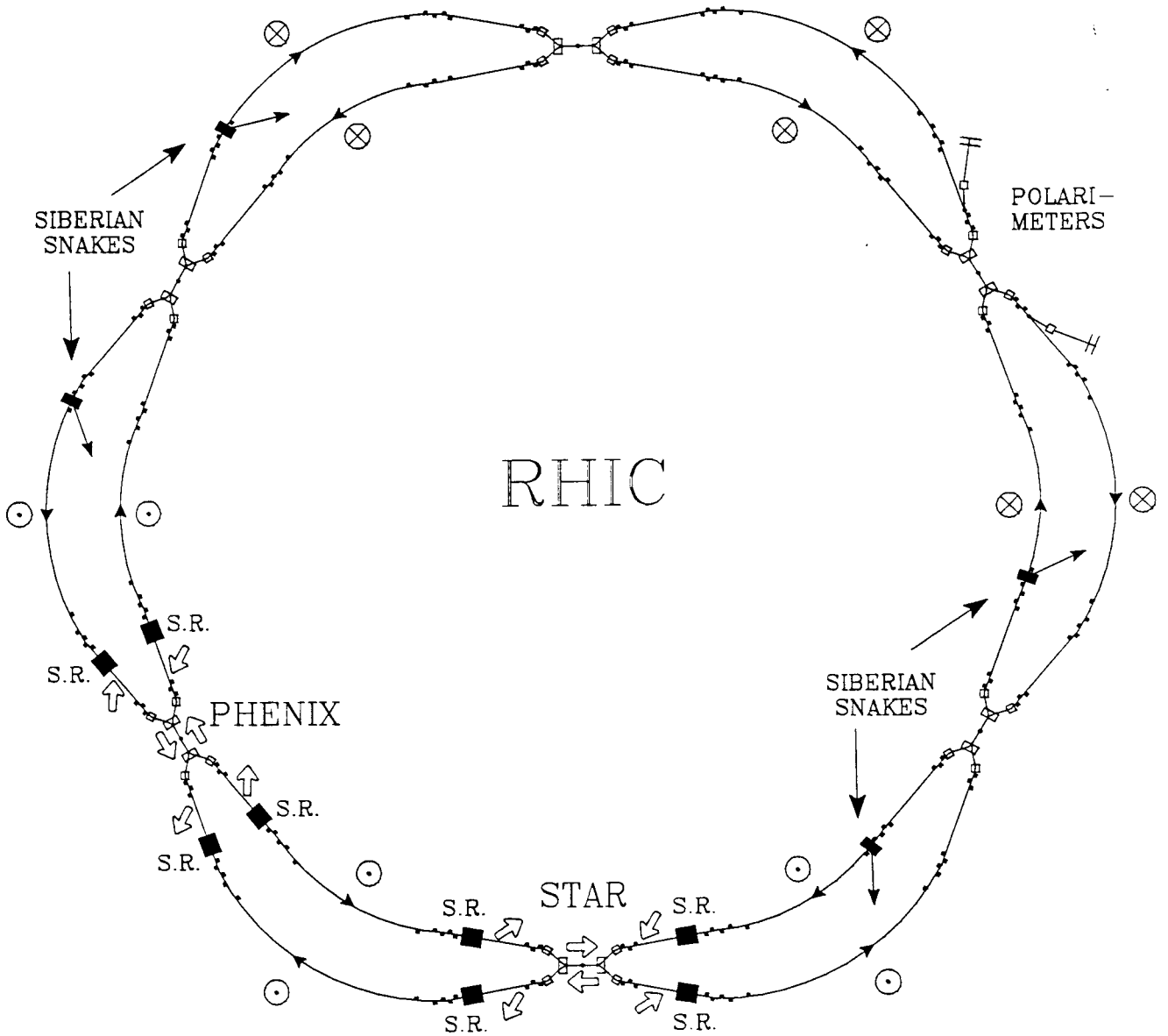
SIBERIAN
SNAKES
POLARI-
METERS
RHIC
S.R.
S.R.
PHENIX
S.R.
S.R.
S.R.
STAR
S.R.
S.R.
S.R.
S.R.
SIBERIAN
SNAKES

Figure 2

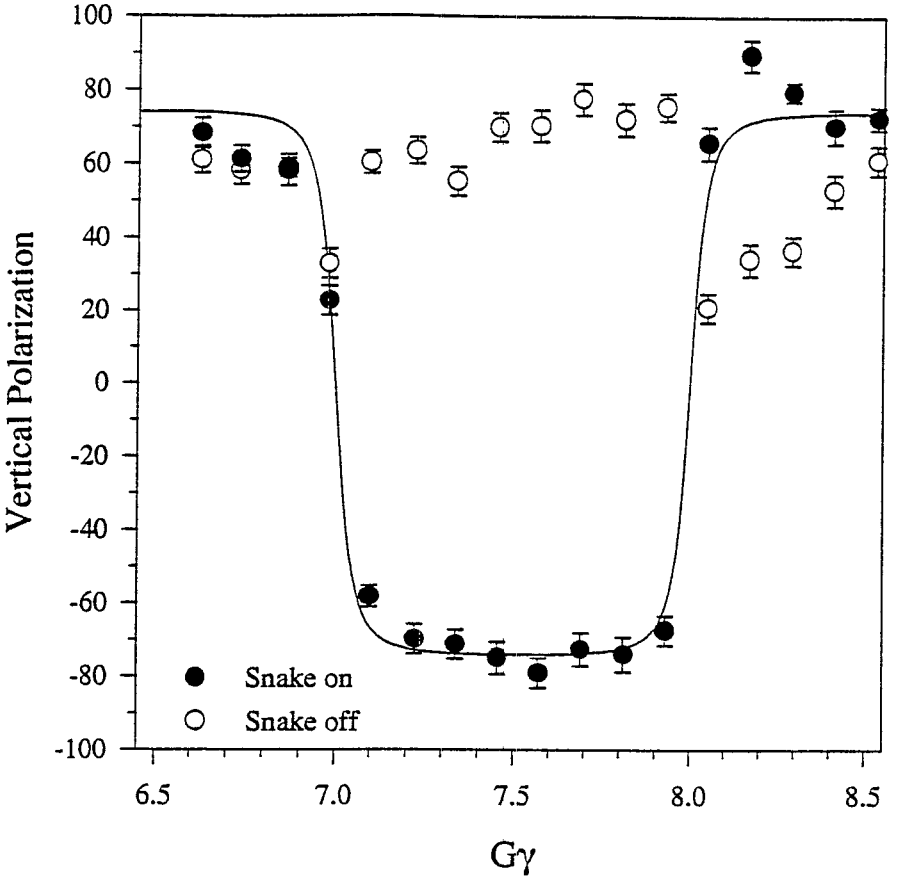
Vertical Polarization
100
80
60
40
20
0
-20
-40
-60
-80
-100
6.5
7.0
7.5
8.0
8.5
Gγ
Snake on
Snake off

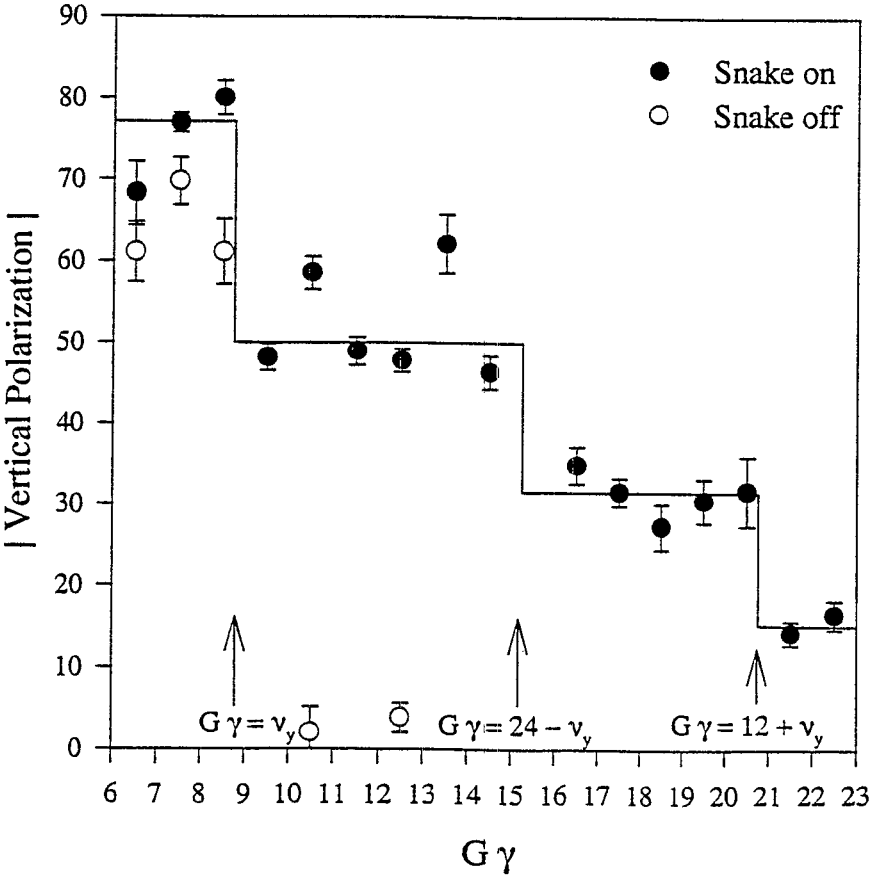
| Vertical Polarization |
90
80
70
60
50
40
30
20
10
0
6 7 8 9 10 11 12 13 14 15 16 17 18 19 20 21 22 23
G γ
Snake on
Snake off
G γ = ν_y
G γ = 24 − ν_y
G γ = 12 + ν_y

Figure 3

PRELIMINARY

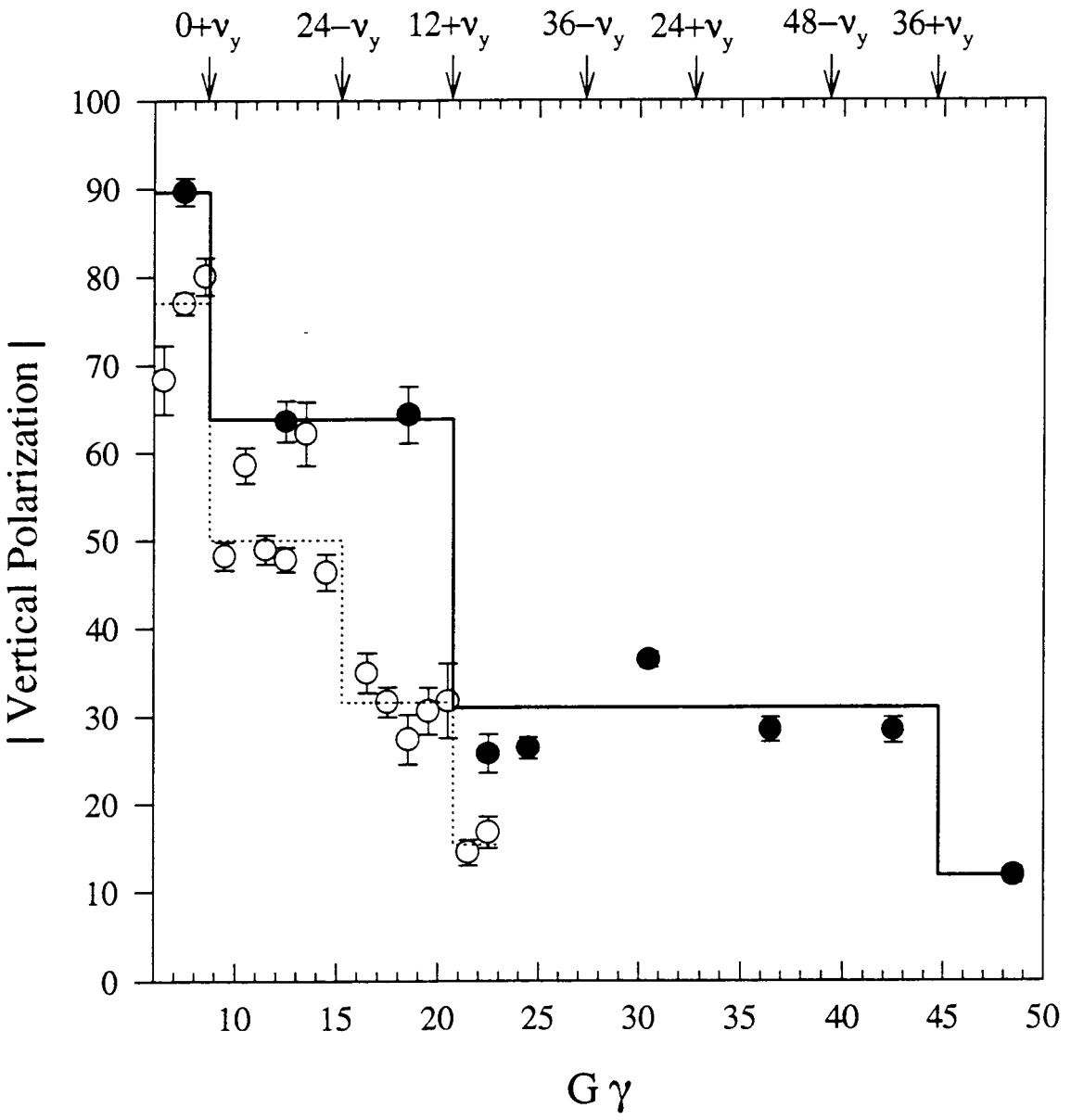

Figure 4

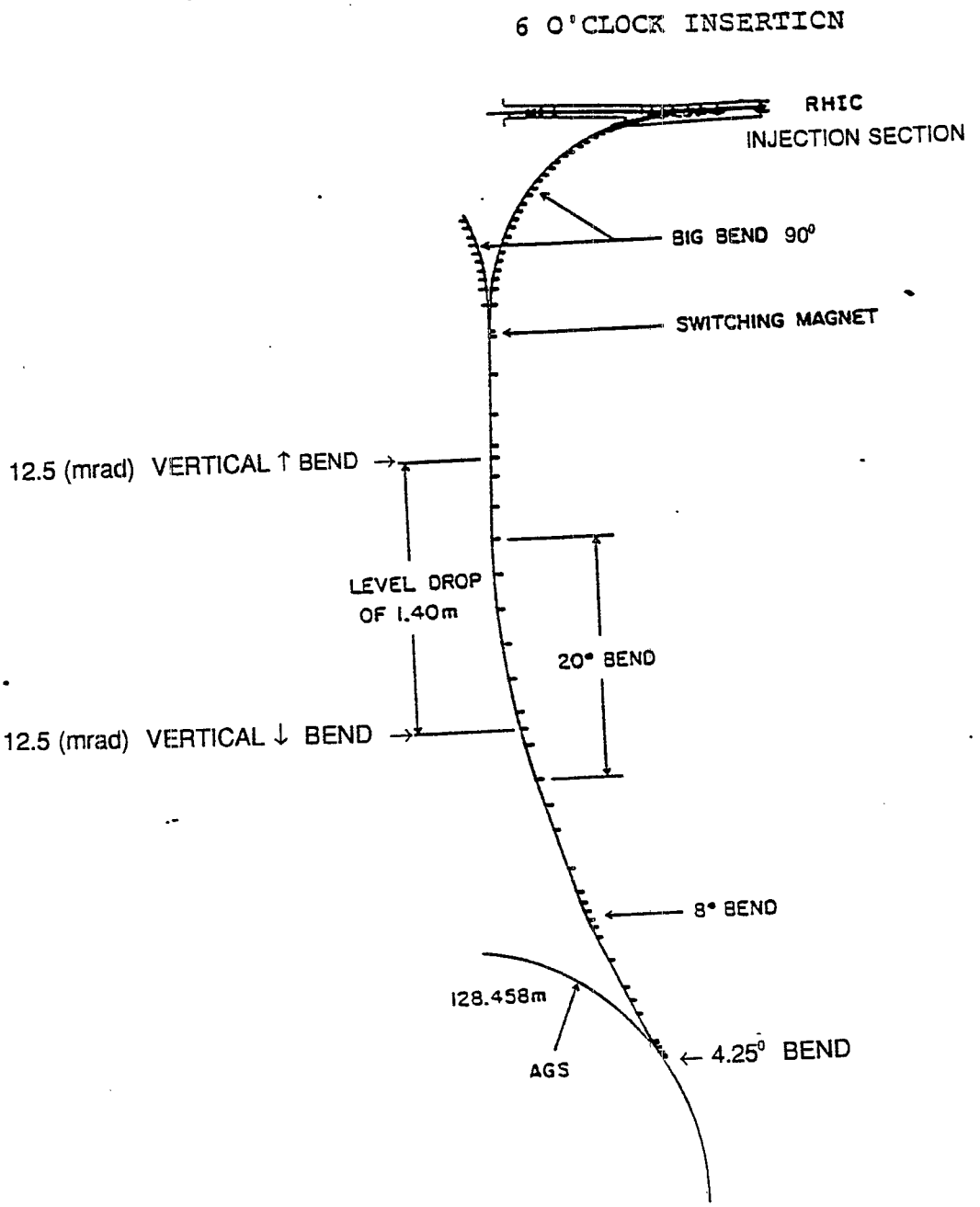

General layout of beam transport system between AGS and RHIC.

Figure 5

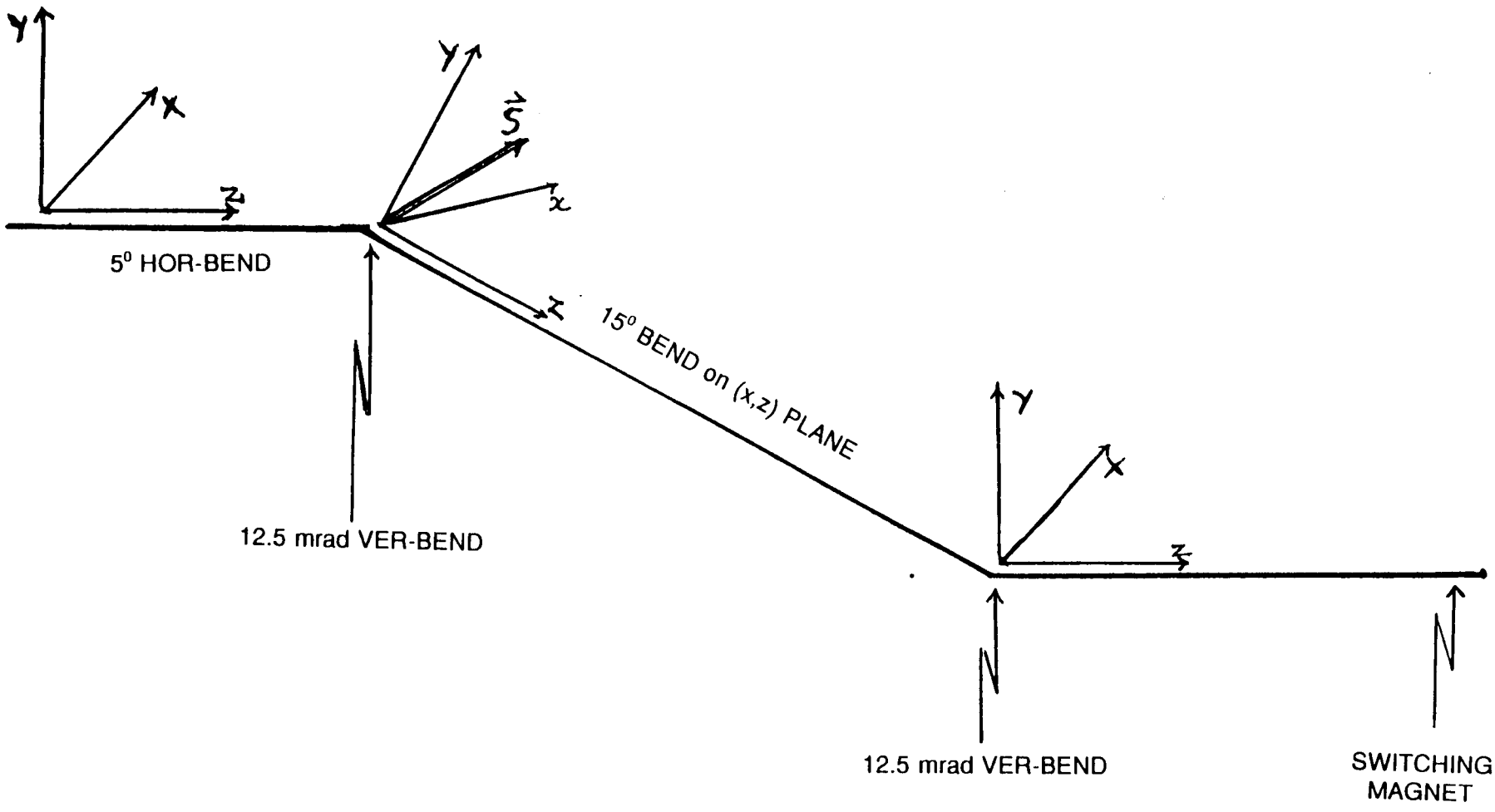

Schematic Diagram of the 20⁰ Bend of the ATR Line. (Bending Magnets only)

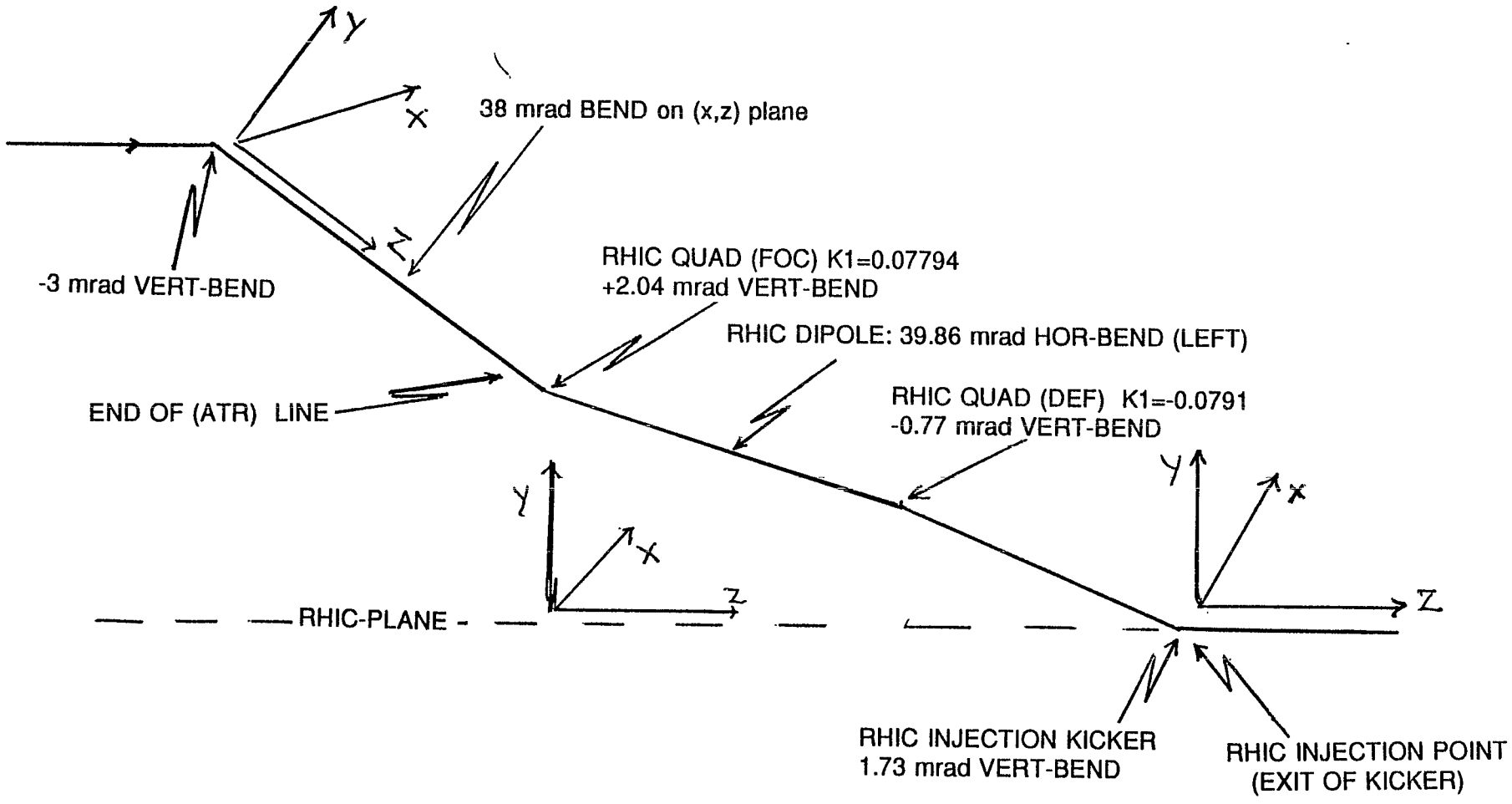

Schematic Diagram of the RHIC Injection Section

Figure 7

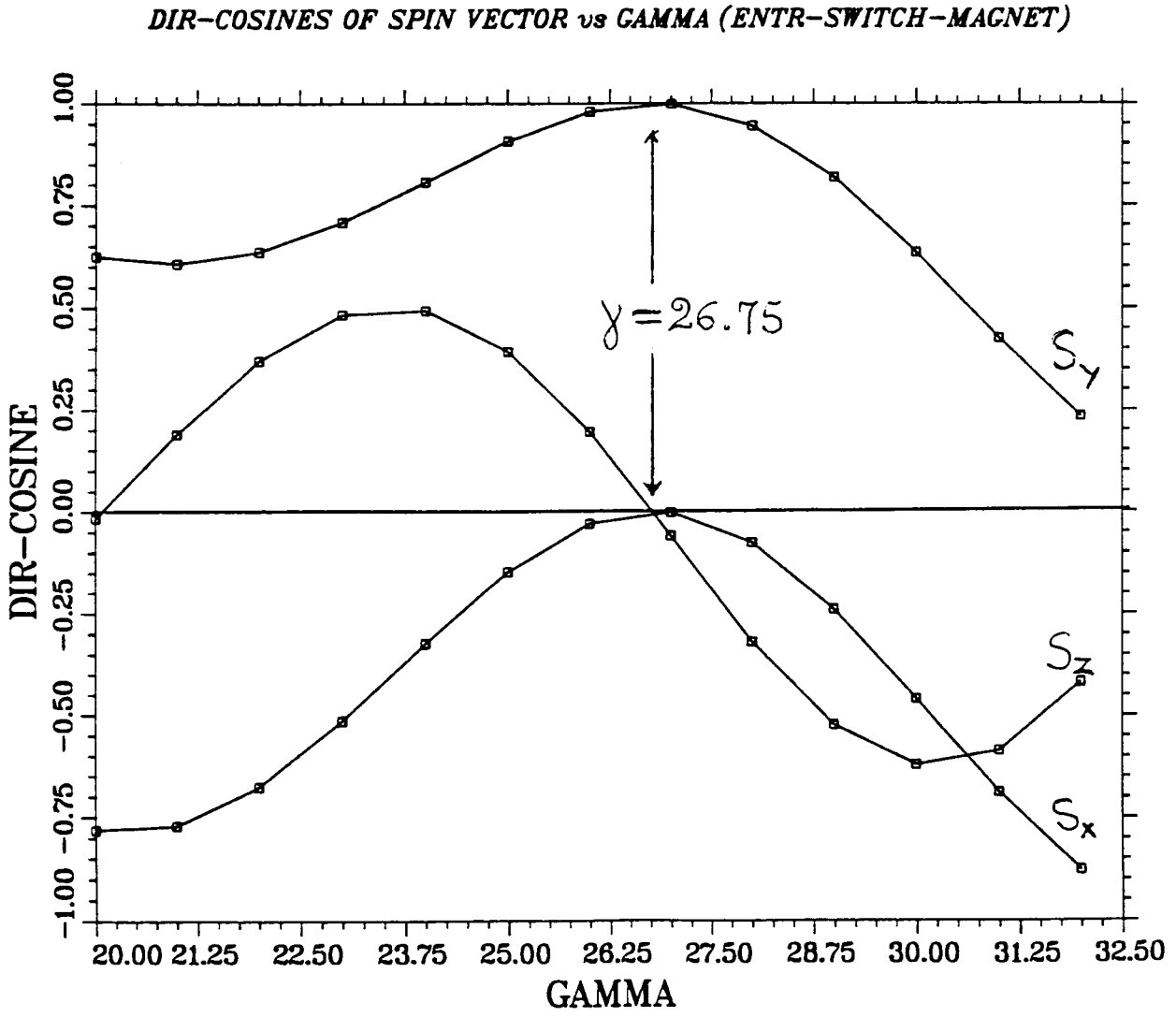

Directional cosines of the proton spin vector, as a function of γ at the entrance of the switching magnet (Fig. 1) , for a central trajectory particle.

Figure 8

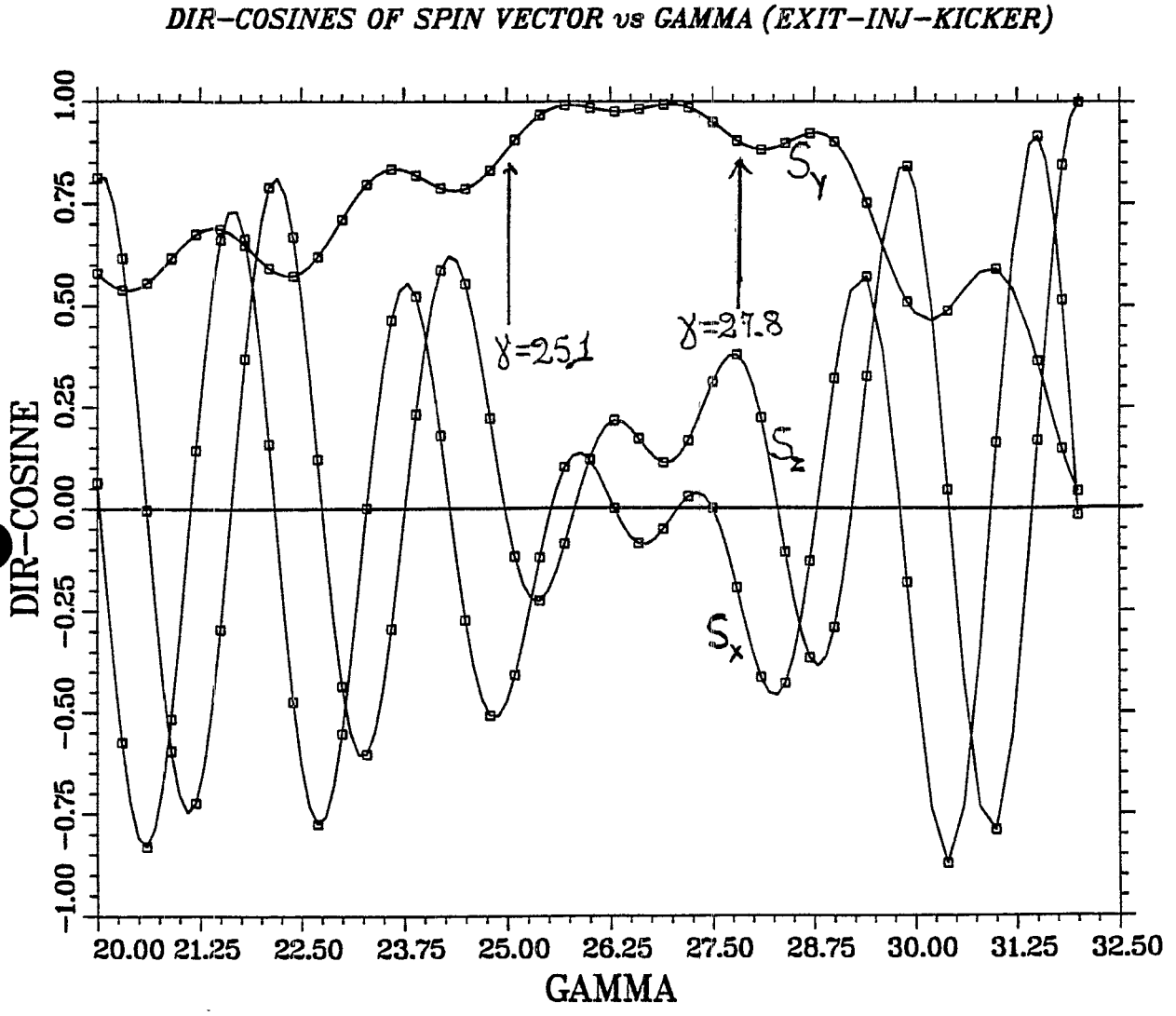

Directional cosines of the proton spin vector, as a function of γ at the RHIC injection point (Fig. 1 & 3) , for a central trajectory particle.

Figure 9

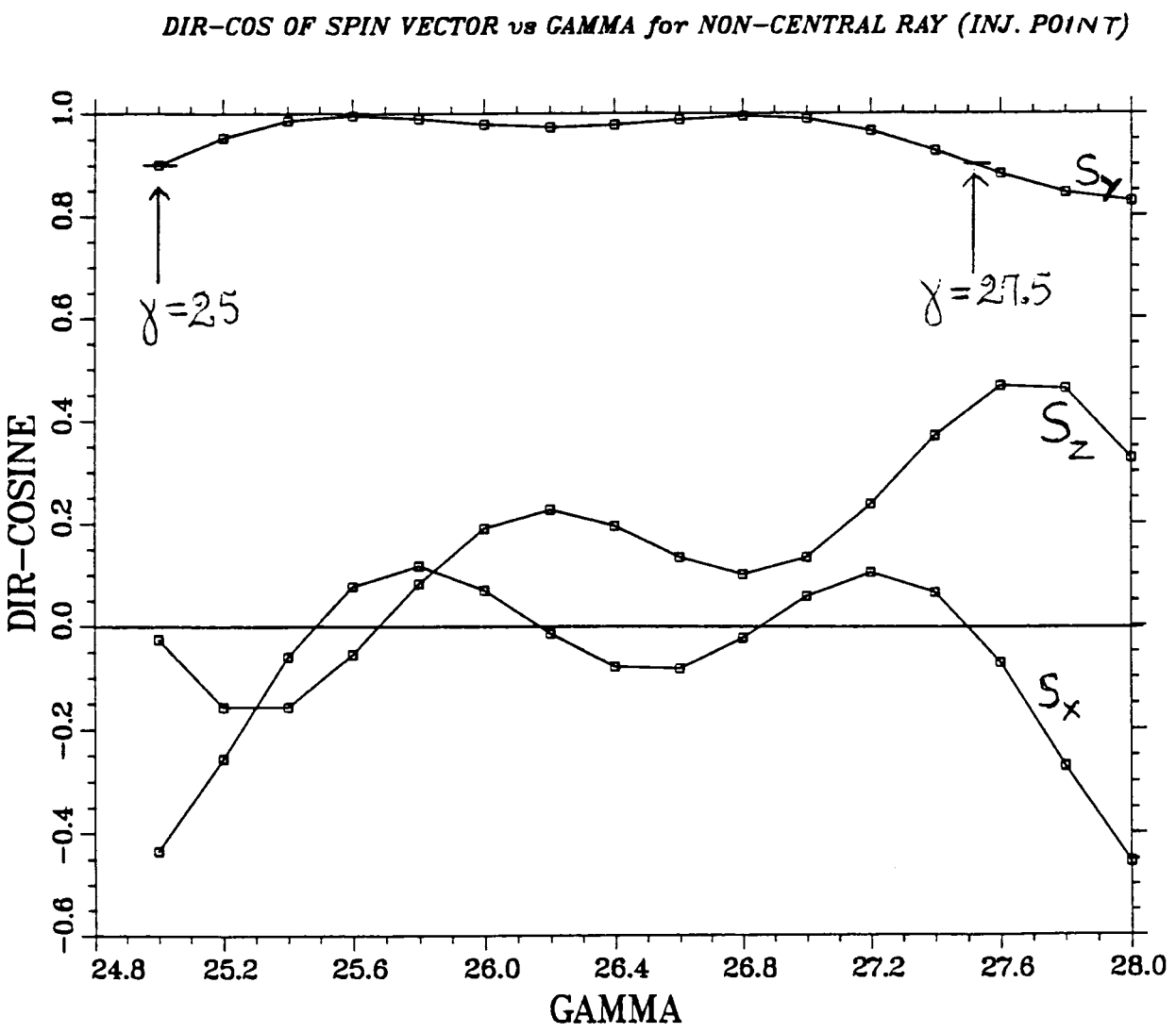

Directional cosines of the proton spin vector, as a function of γ at the RHIC injection point (Fig. 1 & 3) , for a non-central trajectory particle.

Figure 10

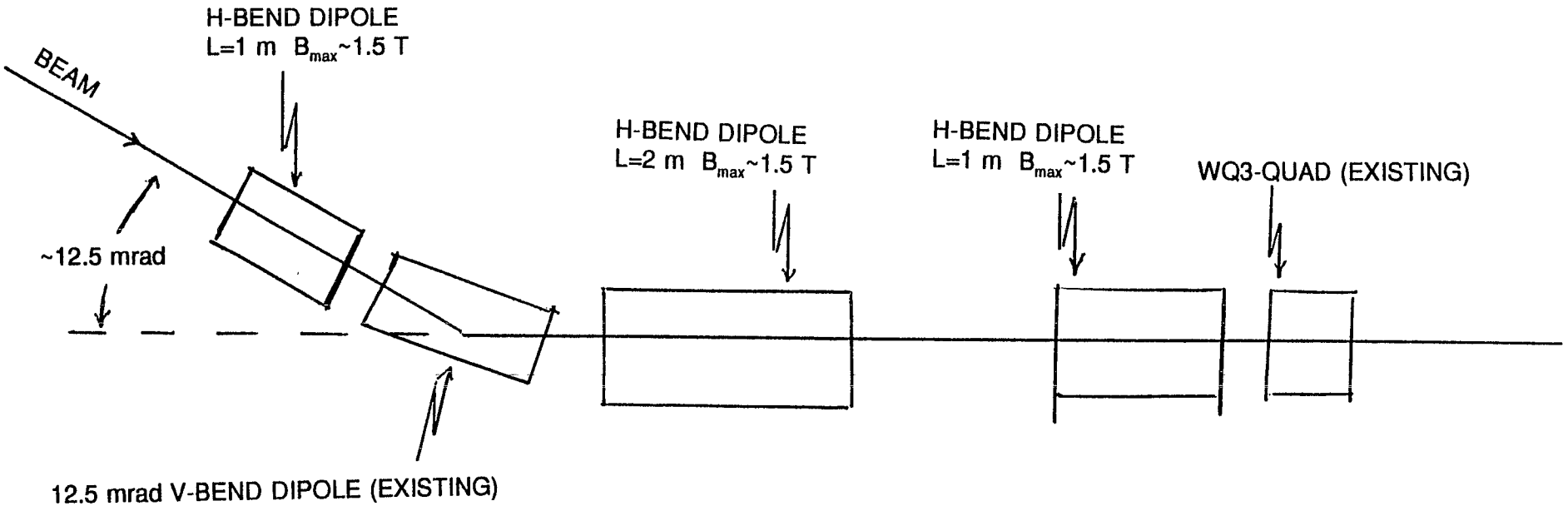

Schematic diagram of the three proposed dipoles showing their relative location with respect to the second vertically bending dipole.

Figure 11

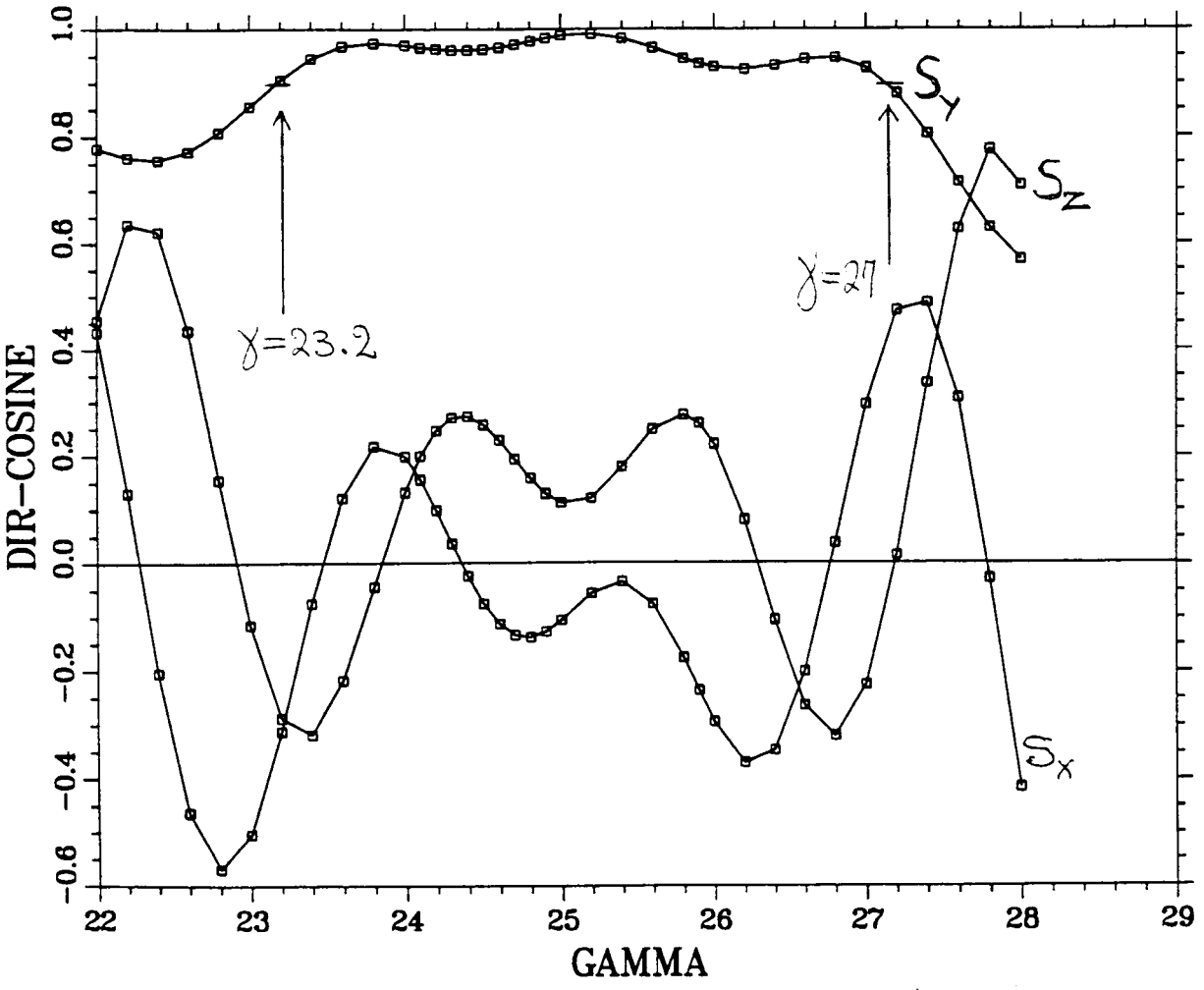

Directional cosines of the proton spin vector, as a function of γ at the RHIC injection point (Fig. 1 & 3) , for central trajectory particles. The first of the three dipole magnets (see text) has been tuned to maximize proton polarization at the entrance of the switching magnet for beam proton energy corresponding to γ=25. The other two dipole restore the central trajectory and cancel the achromaticity introduced by the first dipole.

Figure 12

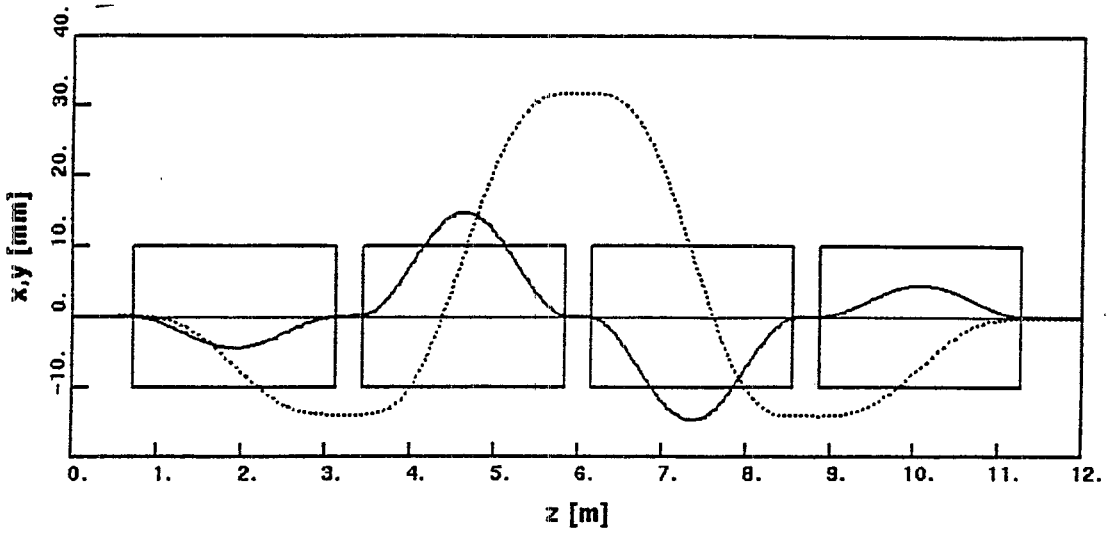
x,y [mm]
40.
30.
20.
10.
0.
-10.
0.
1.
2.
3.
4.
5.
6.
7.
8.
9.
10.
11.
12.
z [m]

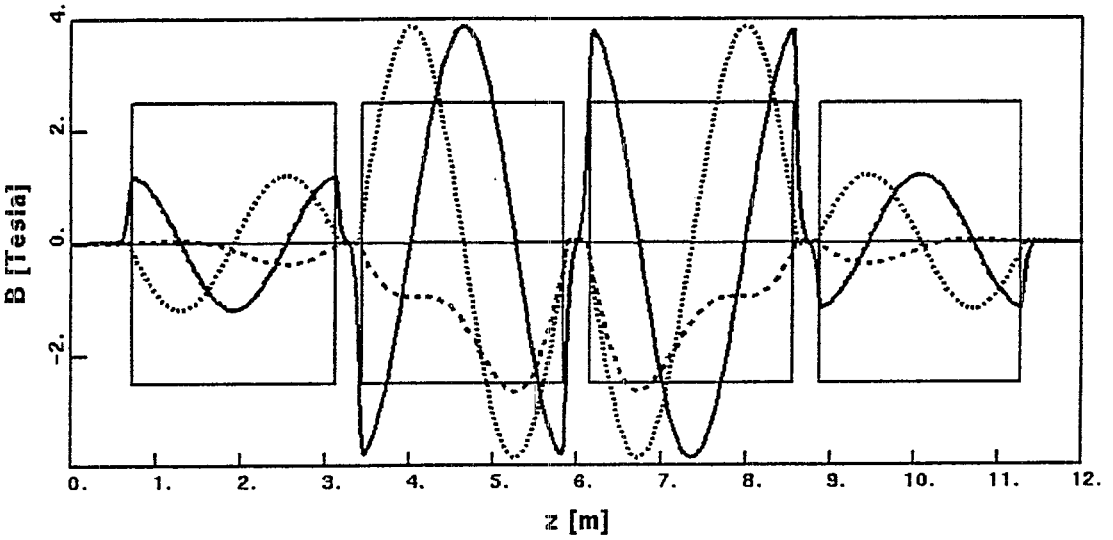
B [Tesla]
4.
2.
0.
-2.
0.
1.
2.
3.
4.
5.
6.
7.
8.
9.
10.
11.
12.
z [m]

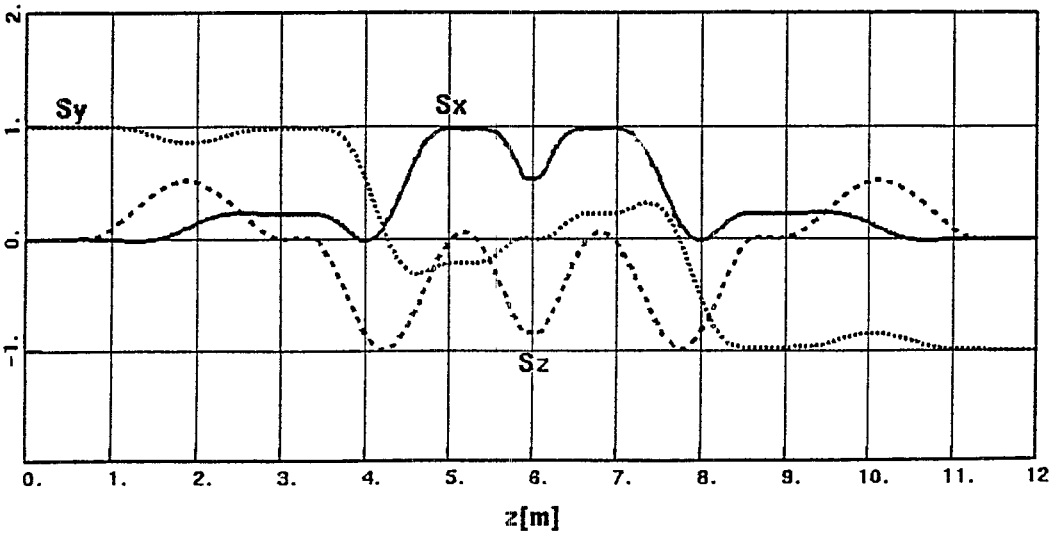
Sy
Sx
Sz
2.
1.
0.
-1.
0.
1.
2.
3.
4.
5.
6.
7.
8.
9.
10.
11.
12
z[m]

Figure 13

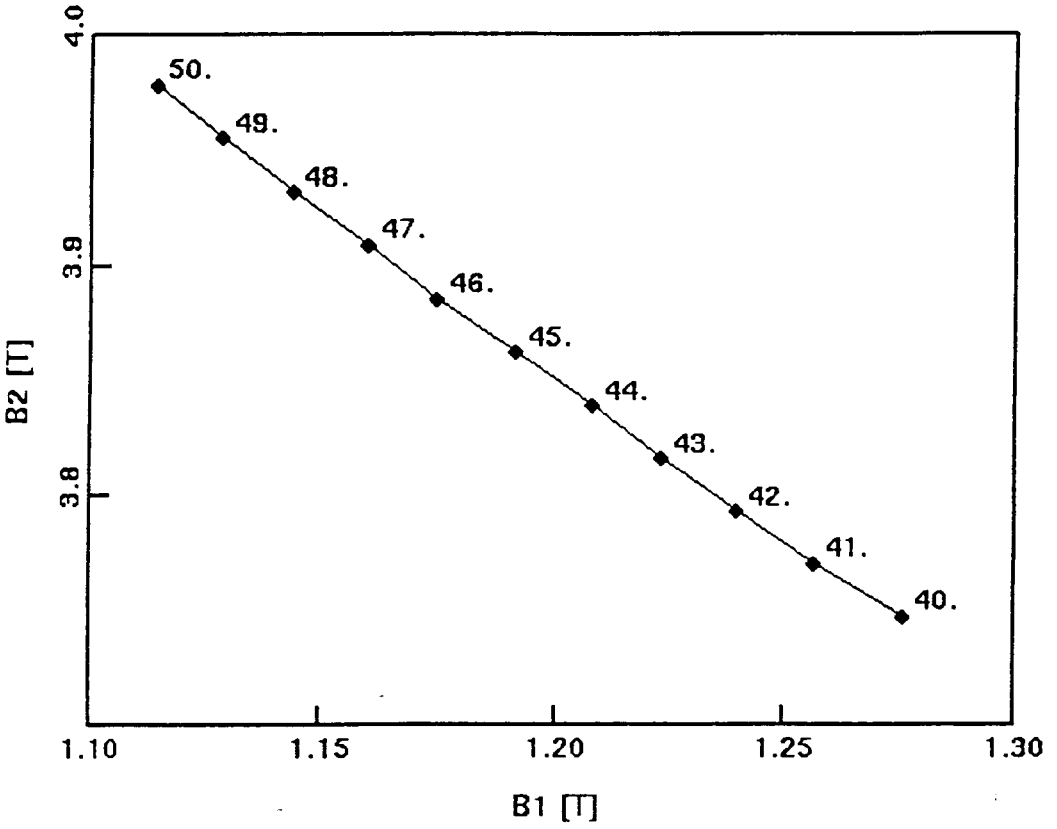

Figure 14

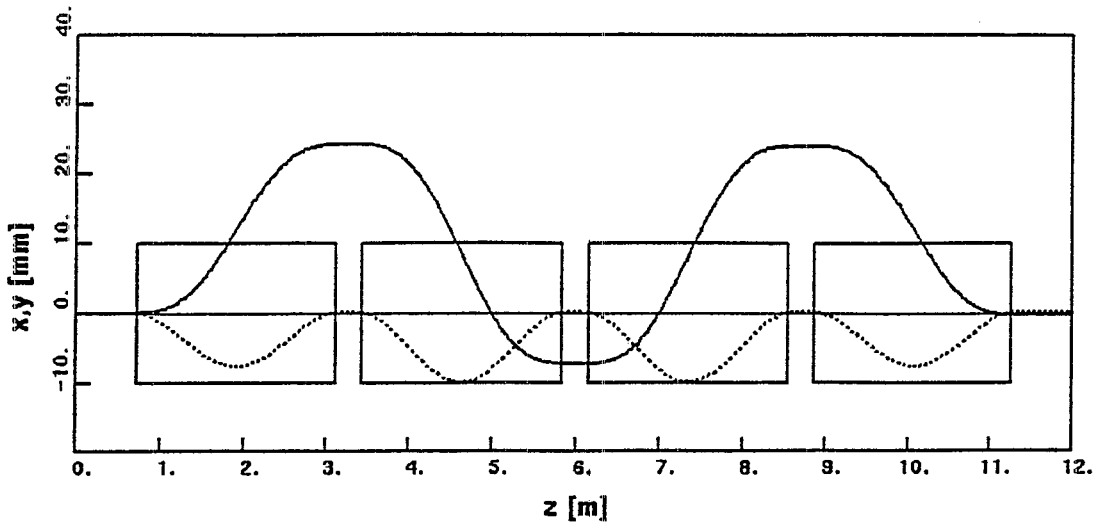
x,y [mm]
40.
30.
20.
10.
0.
-10.
0.
1.
2.
3.
4.
5.
6.
7.
8.
9.
10.
11.
12.
z [m]

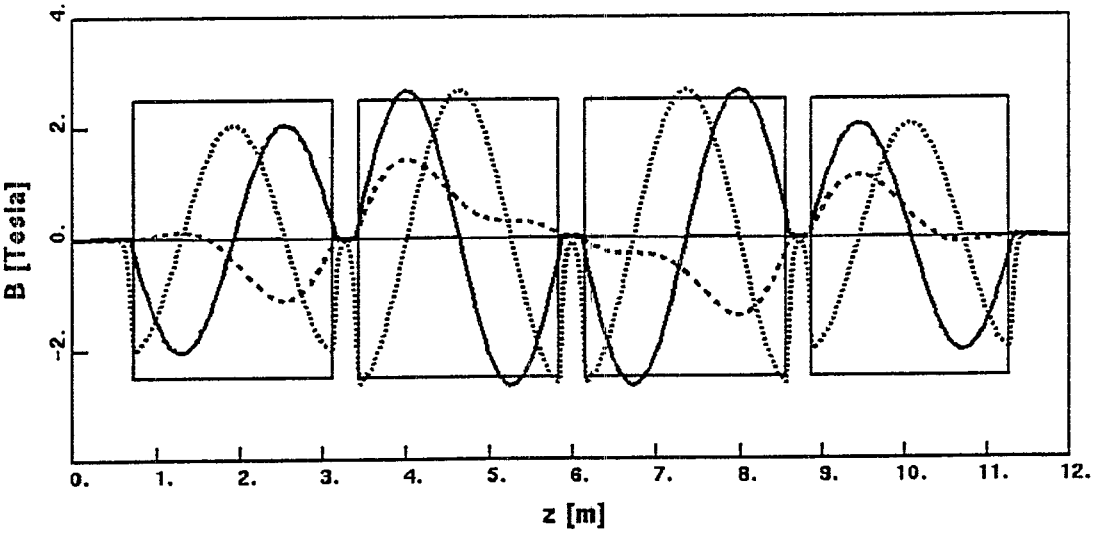
B [Tesla]
4.
2.
0.
-2.
0.
1.
2.
3.
4.
5.
6.
7.
8.
9.
10.
11.
12.
z [m]

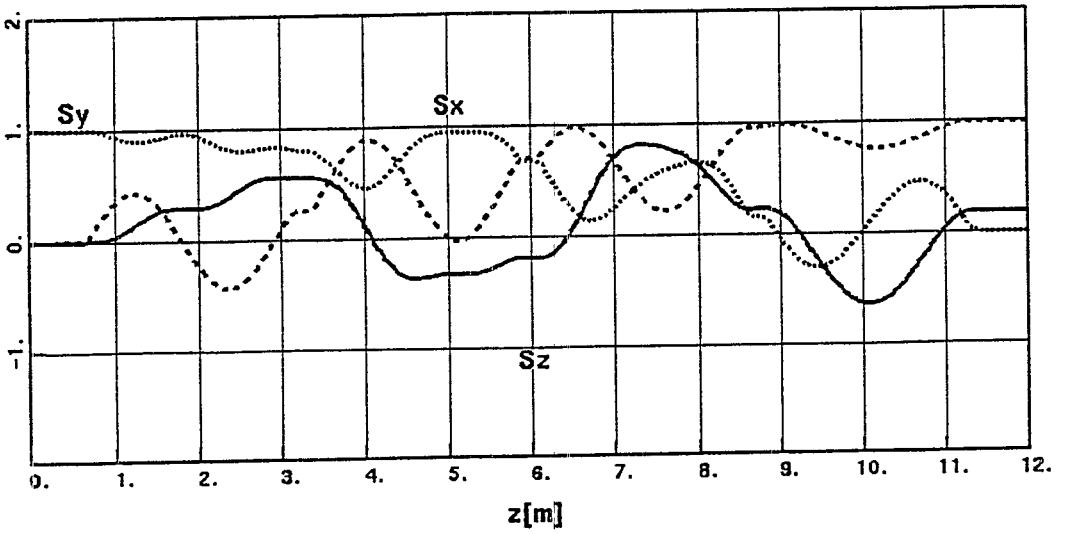
Sy
Sx
Sz
2.
1.
0.
-1.
0.
1.
2.
3.
4.
5.
6.
7.
8.
9.
10.
11.
12.
z[m]

Figure 15

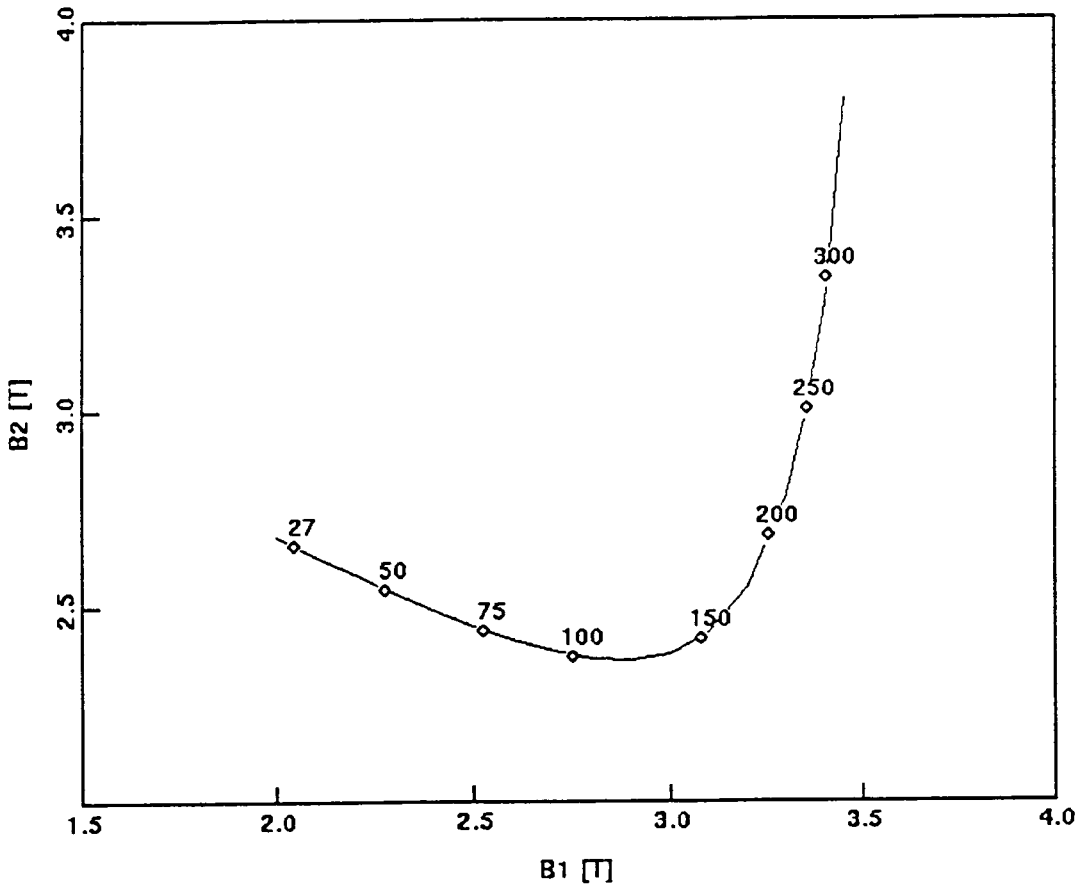

Figure 16

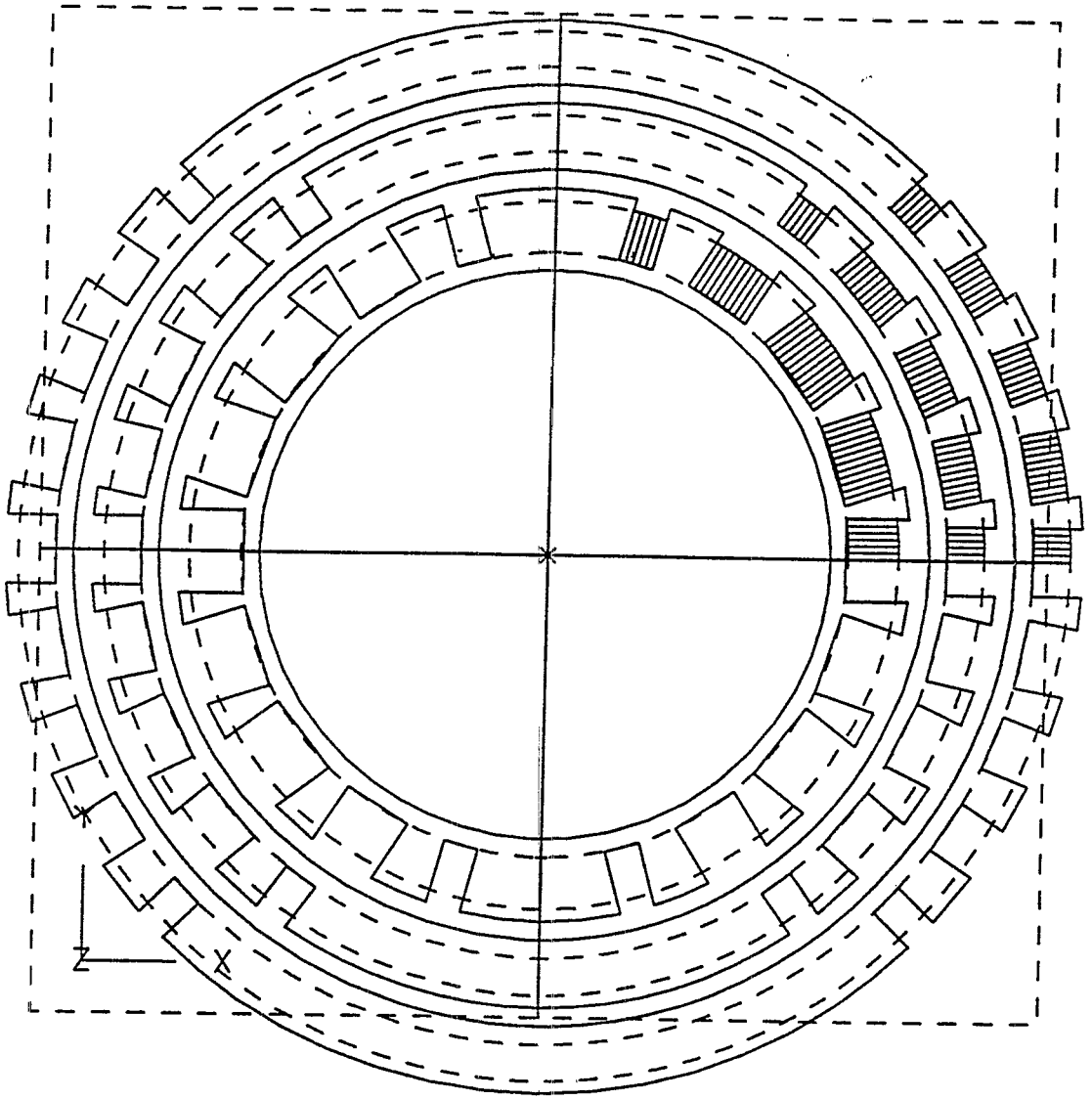

Figure 17

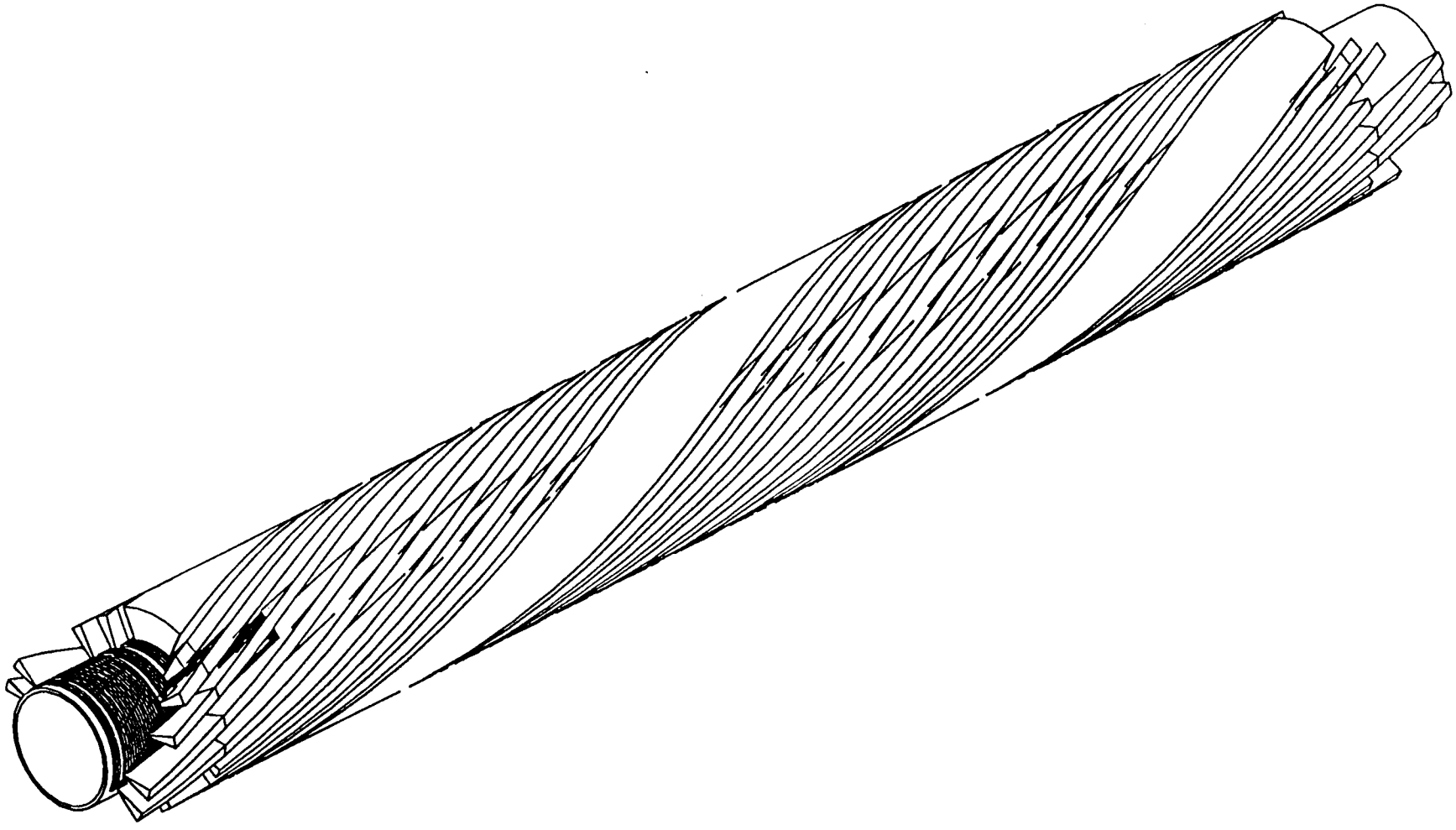

ure 18

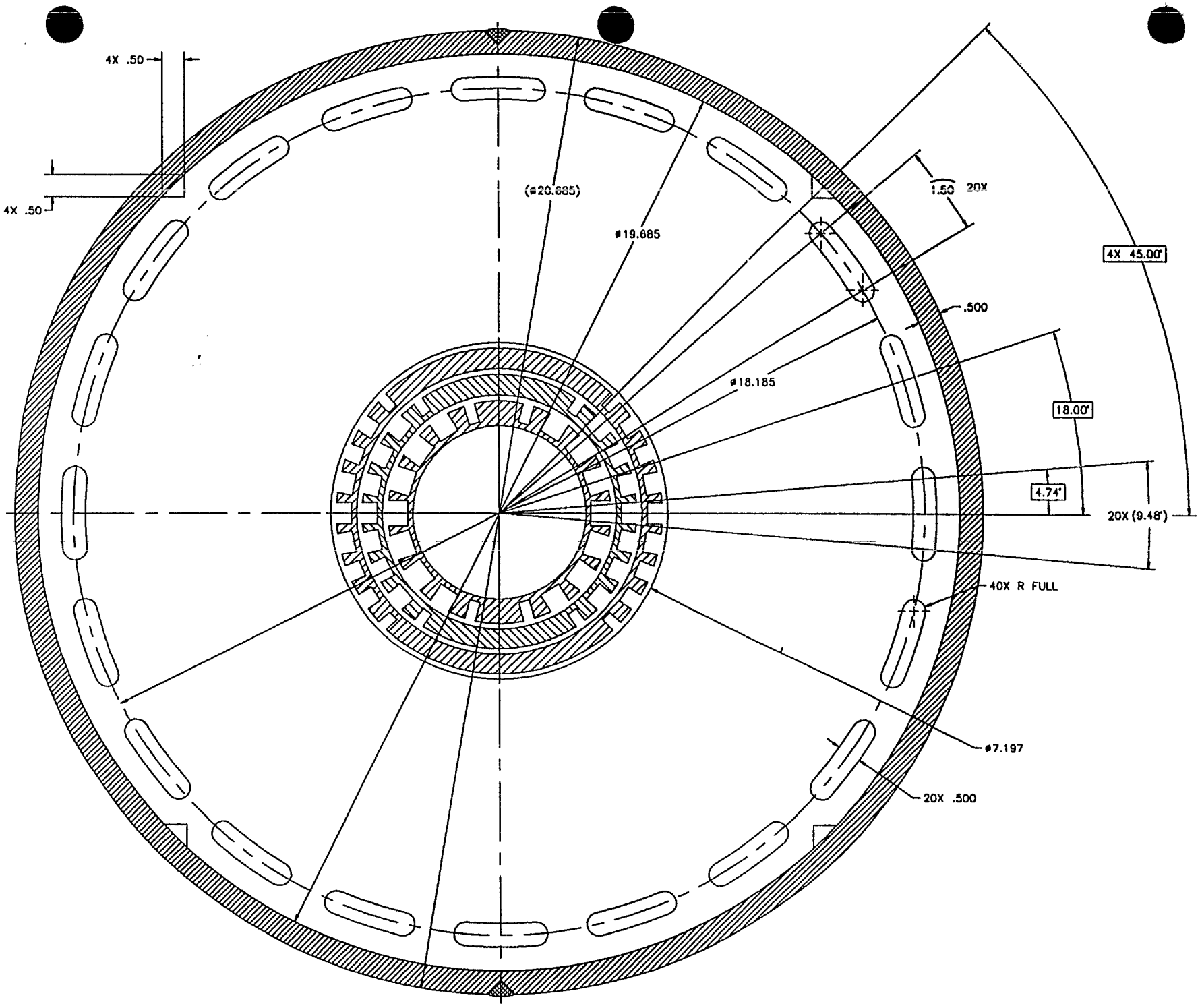
4X .50
4X .50
(ø20.685)
ø19.685
ø18.185
1.50 20X
4X 45.00°
.500
18.00"
4.74"
20X (9.48")
40X R FULL
ø7.197
20X .500

Figure 19

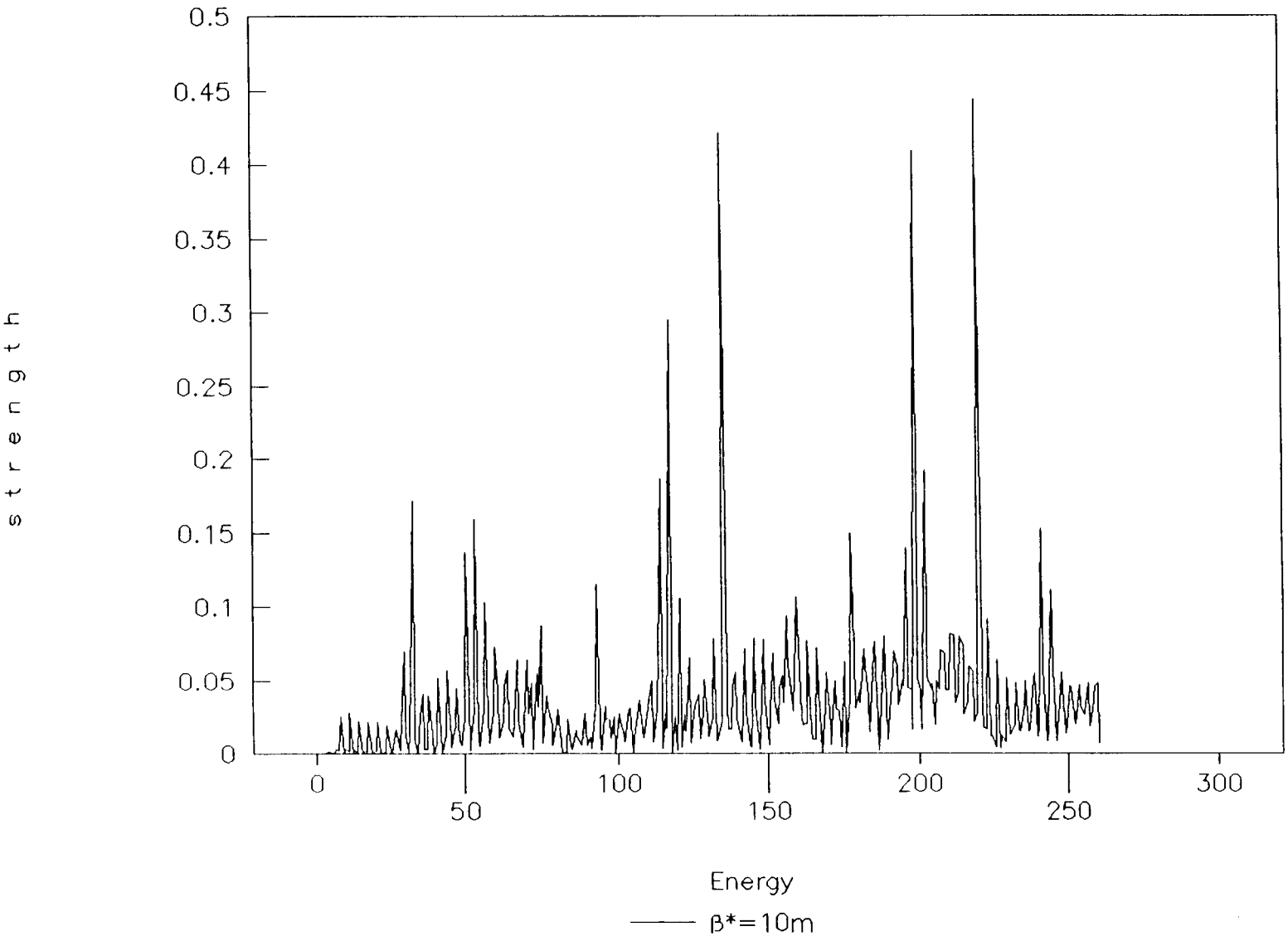
Intrinsic resonance strength
RHIC; invar. emittance 10 μrad-m
strength
0.5
0.45
0.4
0.35
0.3
0.25
0.2
0.15
0.1
0.05
0
0
50
100
150
200
250
300
Energy
β*=10m

ure 20

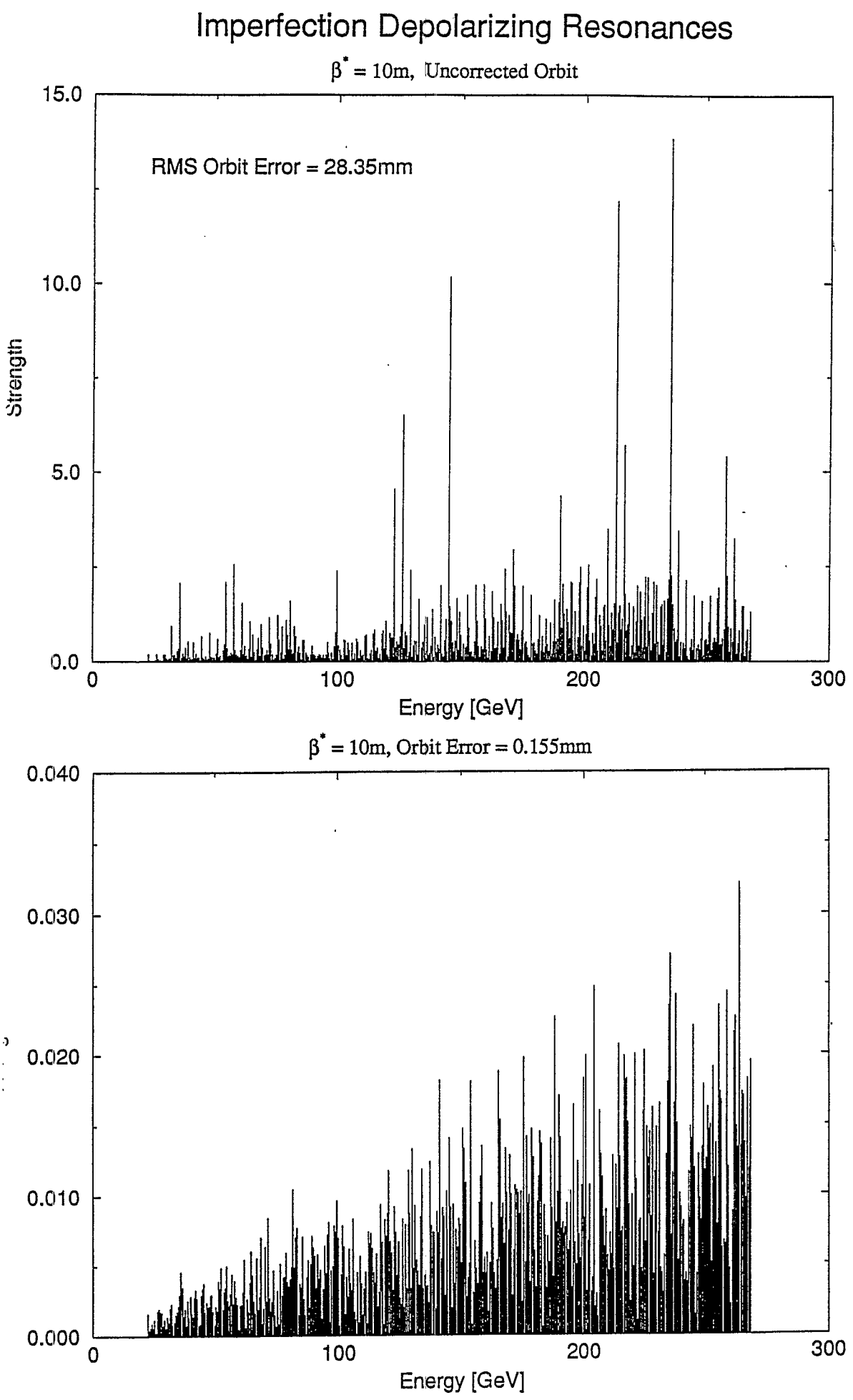
Imperfection Depolarizing Resonances
β* = 10m, Uncorrected Orbit
RMS Orbit Error = 28.35mm
Strength
15.0
10.0
5.0
0.0
0
100
200
300
Energy [GeV]
β* = 10m, Orbit Error = 0.155mm
0.040
0.030
0.020
0.010
0.000
0
100
200
300
Energy [GeV]

Figure 21

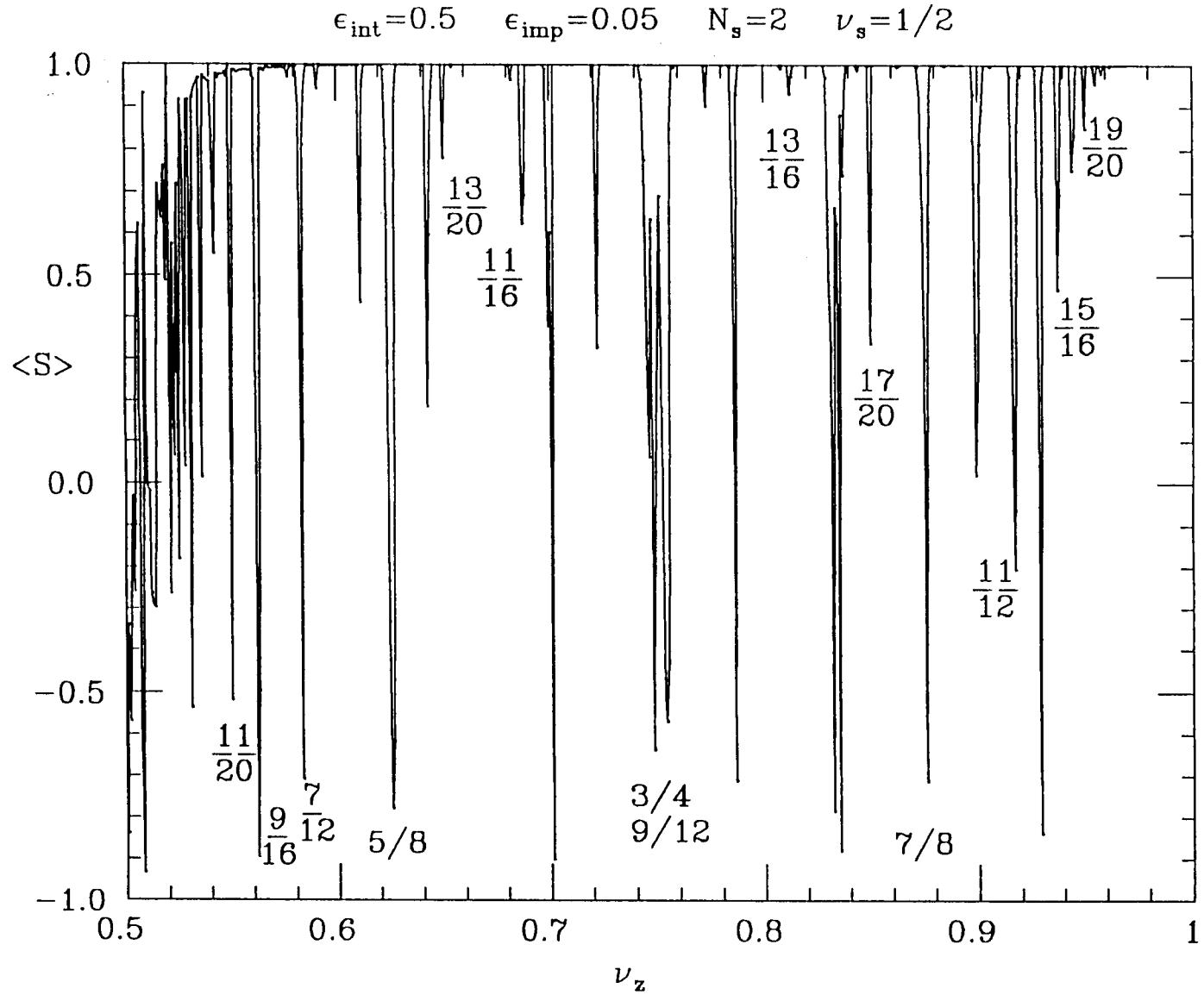
$\epsilon_{int}=0.5$ $\epsilon_{imp}=0.05$ $N_s=2$ $\nu_s=1/2$
1.0
0.5
0.0
−0.5
−1.0
<S>
0.5
0.6
0.7
0.8
0.9
1
ν_z
11/20
9/16
7/12
5/8
13/20
11/16
3/4
9/12
13/16
17/20
7/8
11/12
15/16
19/20

Figure 22

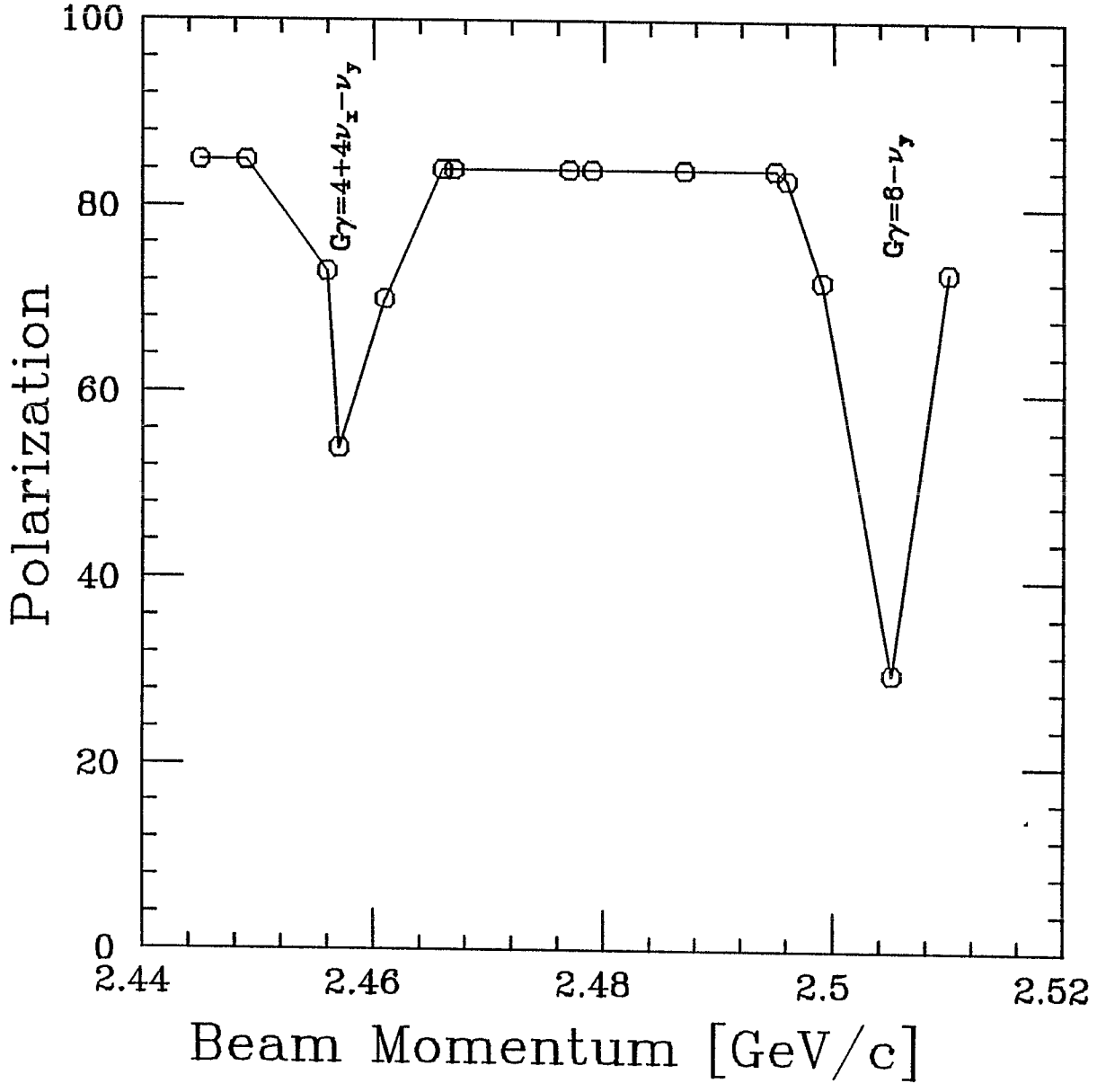
100
80
60
40
20
0
Polarization
2.44
2.46
2.48
2.5
2.52
Beam Momentum [GeV/c]
$G\gamma=4+4\nu_x-\nu_y$
$G\gamma=8-\nu_y$

Figure 23

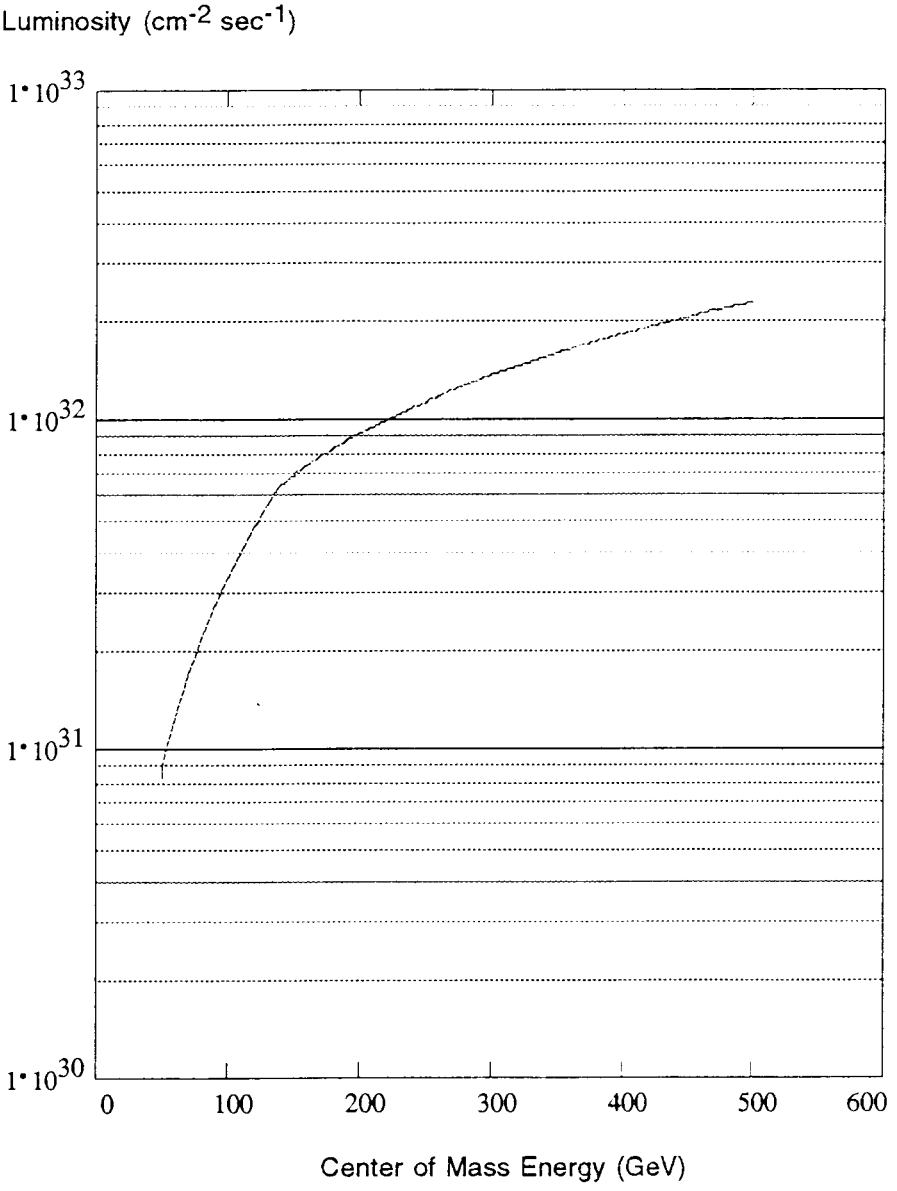
Luminosity (cm-2 sec-1)
1•10^33
1•10^32
1•10^31
1•10^30
0
100
200
300
400
500
600
Center of Mass Energy (GeV)

Figure 24

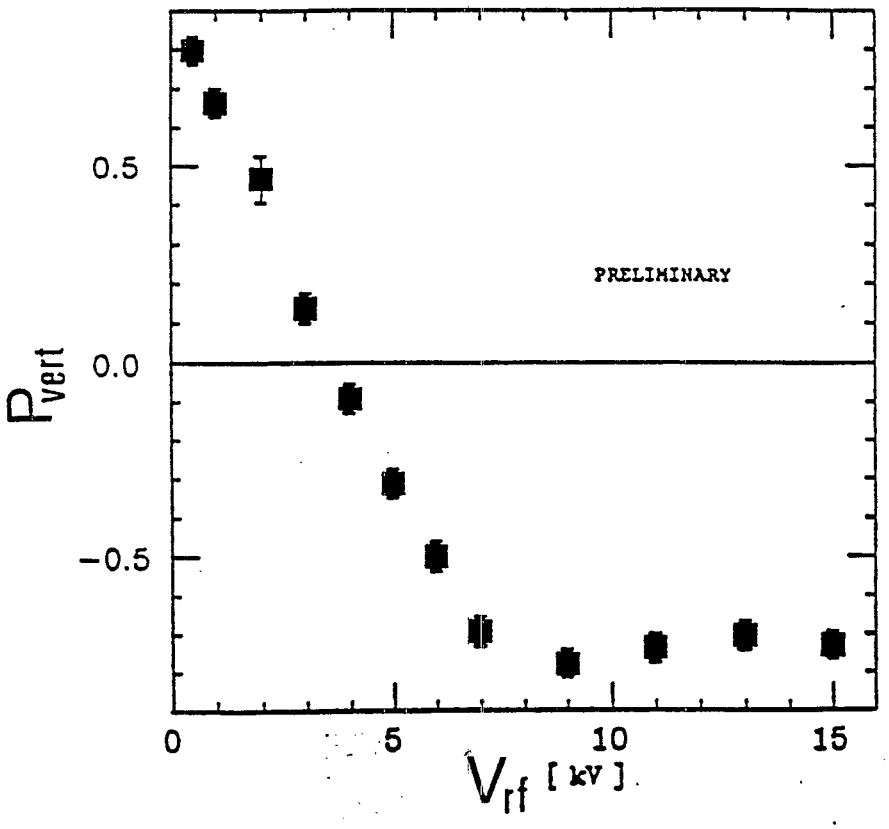

Figure 25

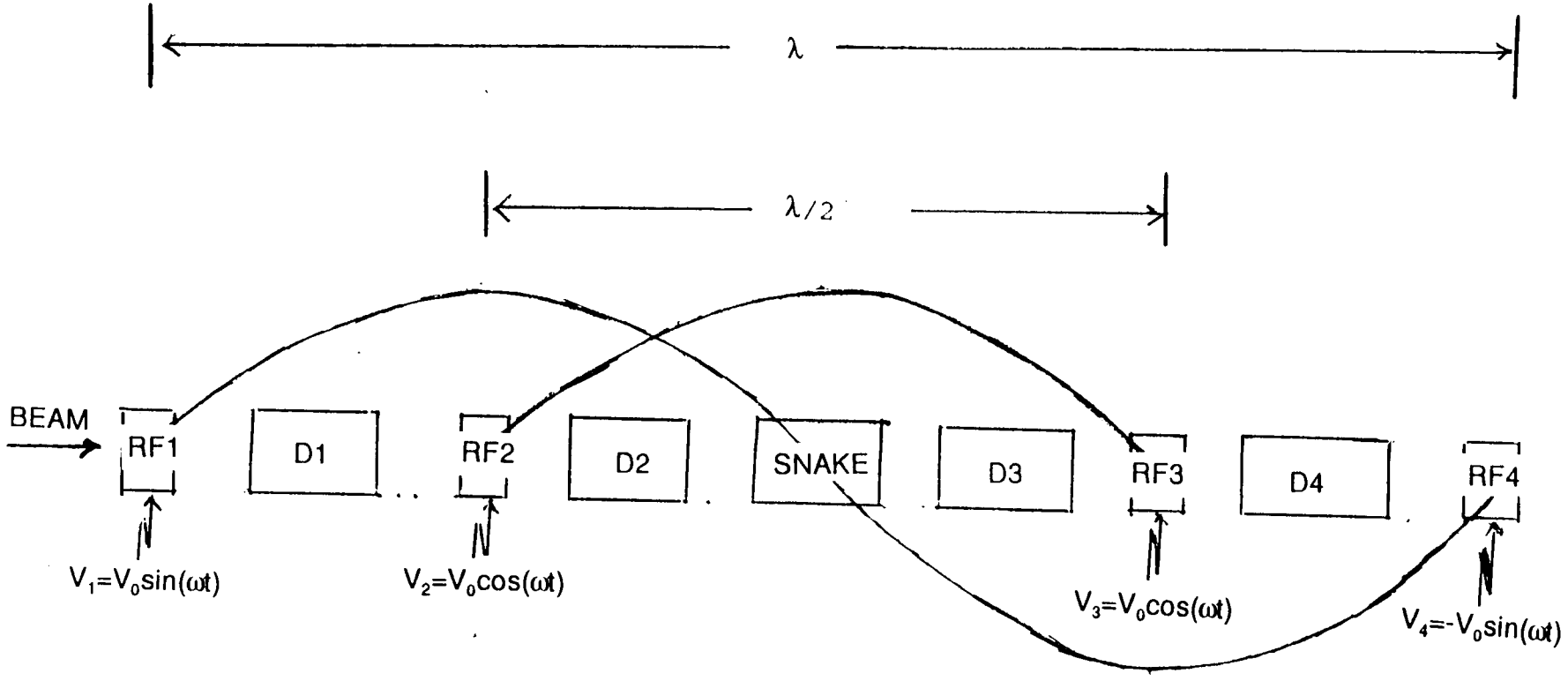

Schematic Diagram of Spin-Flipper with Radio-frequency dipoles and a Siberian Snake.